SIAM J. Applied Dynamical Systems
Vol. 13, No. 4, pp. 1620–1653

Spatiotemporal Dynamics of Neural Fields on Product Spaces*

Paul C. Bressloff† and Samuel R. Carroll†

Abstract. Motivated by the functional architecture of the primary visual cortex, we analyze solutions to a neural field equation defined on the product space $\mathbb{R} \times S^1$, where the circle S^1 represents the orientation preferences of neurons. We show how standard solutions such as orientation bumps in S^1 and traveling wavefronts in $\mathbb{R}$ can destabilize in the presence of this product structure. Using bifurcation theory, we derive amplitude equations describing the spatiotemporal evolution of these instabilities. In the case of destabilization of an orientation bump, we find that synaptic weight kernels representing the patchiness of horizontal cortical connections yield new stable pattern forming solutions. For traveling wavefronts, we find that cross-orientation inhibition induces the formation of a stable propagating orientation bump at the location of the wavefront.

Key words. neural fields, pattern formation, traveling waves, bifurcation theory, visual cortex, integrodifferential equations

AMS subject classification. 92C20

DOI. 10.1137/140976339

1. Introduction.

Understanding the dynamical mechanisms underlying spatially structured activity states in neural tissue is important for a wide range of neurobiological phenomena, both naturally occurring and pathological. For example, a variety of neurological disorders such as epilepsy and spreading depression are characterized by spatially localized oscillations and waves propagating across the surface of the brain (see Chap. 9 of [10]). Moreover, traveling waves can be induced in vitro by electrically stimulating disinhibited cortical slices [17, 39, 41, 56]. Spatially coherent activity states also arise during the normal functioning of the brain, encoding local properties of visual stimuli [47], representing head direction [50], and maintaining persistent activity states in short-term working memory [27, 51]. One of the major challenges in neurobiology is understanding the relationship between spatially structured activity states and the underlying neural circuitry that supports them. This has motivated considerable recent interest in studying reduced continuum neural field models in which the large-scale dynamics of spatially structured networks of neurons is described in terms of nonlinear integrodifferential equations, whose associated integral kernels represent the spatial distribution of neuronal synaptic connections. Such models, which build upon the original work of Wilson and Cowan [54, 55] and Amari [1], provide an important example of spatially extended excitable systems with nonlocal interactions. They can exhibit a rich repertoire of spatiotemporal dynamics, including solitary traveling fronts and pulses, stationary pulses and spatially localized oscillations (breathers), spiral waves, and Turing-like

*Received by the editors July 7, 2014; accepted for publication (in revised form) by B. Ermentrout September 22, 2014; published electronically November 20, 2014.
http://www.siam.org/journals/siads/13-4/97633.html

†Department of Mathematics, University of Utah, Salt Lake City, UT 84112 (bressloff@math.utah.edu, carroll@math.utah.edu).

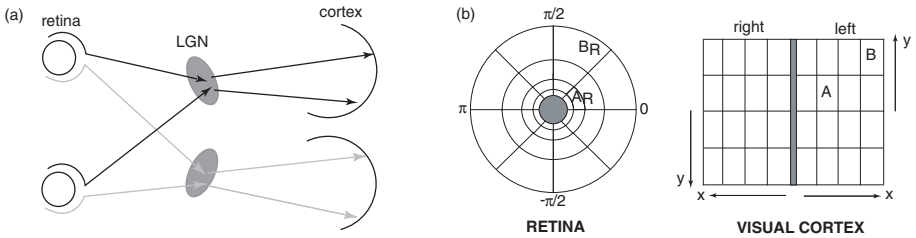

Figure 1. (a) *Visual pathways from the retina through the lateral geniculate nucleus (LGN) of the thalamus to the primary visual cortex (V1).* (b) *Schematic illustration of the complex logarithmic mapping from retina to V1. Foveal region in retina is indicated by shaded disc. Regions A_R and B_R in the visual field are mapped to regions A and B in the cortex.*

patterns [21, 19, 9]. In recent years, neural fields have been used to model a wide range of neurobiological phenomena, including wave propagation in cortical slices [38, 41] and in vivo [29], geometric visual hallucinations [22, 13], EEG rhythms [36, 42, 35, 48], orientation tuning in primary visual cortex (V1) [46, 3, 11], short-term working memory [16, 33], control of head direction [57], motion perception [28], binocular rivalry [14, 52], and the aperture affect in motion vision [40].

One of the simplest neural field models is the scalar integrodifferential equation [54, 55, 1]

$$\tau \frac{\partial u(x,t)}{\partial t} = -u(x,t) + \int_{\mathbb{R}^d} w(x,x')F(u(x',t))\mathrm{d}x', \tag{1.1}$$

where $x' \in \mathbb{R}^d$ with $d = 1, 2$. The neural field $u(x,t)$ represents the local activity of a population of neurons at position x at time t, τ is a synaptic or membrane time constant, w is the distribution of synaptic weights, and F denotes an output firing rate function. A common choice for the firing rate function is a bounded, monotonic function such as a sigmoid,

$$F(u) = \frac{1}{1 + \mathrm{e}^{-\eta(u-\kappa)}}, \tag{1.2}$$

where η is the gain and κ, $\kappa > 0$, is the threshold. In the high gain limit, $\eta \to \infty$, we have $F(u) \to H(u - \kappa)$, where H is the Heaviside function. Even this simple model provides a framework for analyzing a variety of dynamical phenomena including traveling fronts, pattern formation, and stationary bumps, as recently reviewed elsewhere [9]. The types of spontaneous spatiotemporal dynamics supported by the neural field depends on the particular structure of the weight distribution w and the threshold/gain of the sigmoid function. Typically, w is taken to depend on the distance $|x - x'|$ between presynaptic and postsynaptic neuronal populations, so that the neural field model is homogeneous (and isotropic when $d = 2$). However, the functional architecture of a cortical region such as the primary visual cortex (V1) suggests that the synaptic weights are far from homogeneous. In order to highlight this point, it is worthwhile to review briefly the structure of V1.

V1 is the first cortical area to receive visual information from the retina (see Figure 1(a)). The output from the retina is conveyed by ganglion cells whose axons form the optic nerve. The optic nerve conducts the output spike trains of the retinal ganglion cells to the lateral

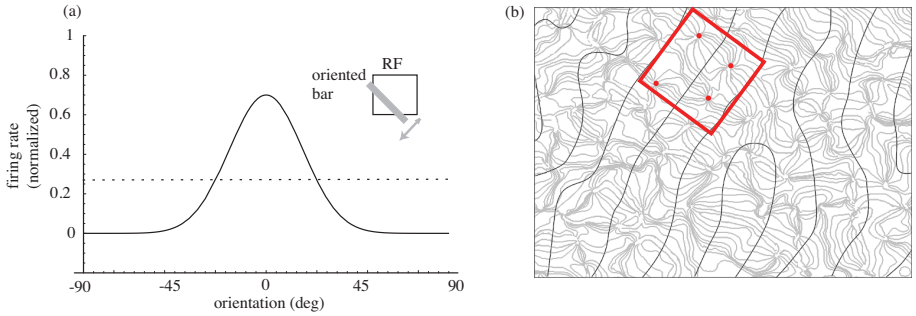

Figure 2. (a) *Schematic illustration of an orientation tuning curve of a V1 neuron. Average firing rate is plotted as a function of the orientation of a bar stimulus that is moved back and forth within the receptive field (RF) of the neuron. The peak of the orientation tuning curve corresponds to the orientation preference of the cell.* (b) *Schematic illustration of iso-orientation (light) and ocular dominance (dark) contours in a region of primate V1. A cortical hypercolumn consists of two orientation singularities or pinwheels per ocular dominance column.*

geniculate nucleus (LGN) of the thalamus, which acts as a relay station between retina and primary visual cortex (V1). Prior to arriving at the LGN, some ganglion cell axons cross the midline at the optic chiasm. This allows the left and right sides of the visual fields from both eyes to be represented on the right and left sides of the brain, respectively. Note that signals from the left and right eyes are segregated in the LGN and in input layers of V1. This means that the corresponding LGN and cortical neurons are monocular, in the sense that they only respond to stimuli presented to one of the eyes but not the other (ocular dominance). One of the striking features of the early visual system is that the visual world is mapped onto the cortical surface in a topographic manner. This means that neighboring points in a visual image evoke activity in neighboring regions of the visual cortex. Moreover, one finds that the central region of the visual field has a larger representation in V1 than the periphery, partly due to a nonuniform distribution of retinal ganglion cells. The retinotopic map is defined as the coordinate transformation from points in the visual world to locations on the cortical surface and can be approximated by a complex logarithm [45]; see Figure 1(b). Superimposed upon the retinotopic map are additional maps reflecting the fact that neurons respond preferentially to stimuli with particular features [49]. For example, one finds that most V1 cells respond preferentially to stimuli with certain preferred orientations (see Figure 2). Over the past 20 years much information has accumulated about the spatial distribution of orientation selective cells in V1. One finds that orientation preferences rotate smoothly over the surface of V1 and that cells with similar feature preferences tend to arrange themselves in vertical columns so that to a first approximation the layered structure of the cortex can be ignored. A more complete picture of the two-dimensional distribution of both orientation preference and ocular dominance in layers 2/3 has been obtained using optical imaging techniques [5, 6, 4]. The basic experimental procedure involves shining light directly onto the surface of the cortex. The degree of light absorption within each patch of cortex depends on the local level of activity. Thus, when an oriented image is presented across a large part of the visual field, the regions of cortex that are particularly sensitive to that stimulus will be differentiated. The topography revealed by these methods has a number of

characteristic features [37]; see Figure 2(b): (i) Orientation preference changes continuously as a function of cortical location, except at singularities or *pinwheels*. (ii) There exist *linear zones*, approximately 750×750 μm^2 in area (in primates), bounded by pinwheels, within which iso-orientation regions form parallel slabs. (iii) Linear zones tend to cross the borders of ocular dominance stripes at right angles; pinwheels tend to align with the centers of ocular dominance stripes. These experimental findings suggest that there is an underlying periodicity in the microstructure of V1 with a period of approximately 1 mm (in cats and primates). The fundamental domain of this approximate periodic (or quasi-periodic) tiling of the cortical plane is the hypercolumn [30, 31, 34], which contains two sets of orientation preferences $\theta \in [0, \pi)$ per eye, organized around a pair of singularities; see Figure 2(b). Within each hypercolumn, neurons with sufficiently similar orientations tend to excite each other, whereas those with sufficiently different orientations inhibit each other, and this serves to sharpen a particular neuron's orientation preference [3]. Moreover, anatomical evidence suggests that longer-range, patchy horizontal and feedback connections link neurons in different hypercolumns, provided that they have similar orientation preferences [2].

One of the immediate implications of the existence of regularly repeating feature maps and patchy horizontal (or feedback) connections is that we can no longer treat the weight distribution w in the neural field equation (1.1) as homogeneous. That is, we have to consider a more general weight distribution of the form (ignoring anisotropies [13])

$$w(x, x') = w(\theta(x) - \theta(x'))J(|x - x'|), \tag{1.3}$$

where $\theta(x)$ denotes an orientation preference map and J represents the dependence of patchy horizontal connections on the orientation preferences of the presynaptic and postsynaptic neuron populations. (One could also incorporate other feature preference maps such as ocular dominance and spatial frequency [8] or variables associated with texture processing [18].) One of the difficulties in modeling synaptic weights according to (1.3) is that it is necessary to specify the preference map $\theta(x)$, which has a nontrivial dependence on position x. This has motivated an alternative class of cortical models, in which each hypercolumn is collapsed into a single point (through some form of spatial coarse-graining) and V1 is treated as a continuum of hypercolumns [13, 12, 11]. Thus cortical position x is replaced by the pair $\{x, \theta\}$ with $x \in \mathbb{R}^d$ now labeling the hypercolumn at (coarse-grained) position x and $\theta, -\pi/2 < \theta \leq \pi/2$, labeling the orientation preferences of neurons within the hypercolumn. Let $u(x, \theta, t)$ denote the activity of a neuronal population at (x, θ), and suppose that u evolves according to the generalized neural field equation

$$\tau \frac{\partial u(x, \theta, t)}{\partial t} = -u(x, \theta, t) + \int_{\mathbb{R}^d} \int_{-\pi/2}^{\pi/2} w(x, \theta | x', \theta') F(u(x', \theta', t)) d\theta' dx'. \tag{1.4}$$

Moreover, the weight distribution now has the independent product form

$$w(x, \theta | x', \theta') = w(\theta - \theta')J(|x - x'|) \tag{1.5}$$

so that the neural field equation reduces to

$$\tau \frac{\partial u(x, \theta, t)}{\partial t} = -u(x, \theta, t) + \int_{\mathbb{R}^d} \int_{-\pi/2}^{\pi/2} w(\theta - \theta')J(|x - x'|) F(u(x', \theta', t)) d\theta' dx'. \tag{1.6}$$

We thus recover a homogeneous neural field in a higher-dimensional space given by the product space $\mathbb{R}^d \times S^1$, where S^1 is the circle. Equation (1.6) is known as a coupled ring model and has previously been used to study geometric visual hallucinations [13, 7] and stimulus-driven contextual effects in visual processing [11, 44]. In particular, the effects of pattern-forming instabilities of a stationary, homogeneous (x and θ independent) solution have been investigated using weakly nonlinear analysis and bifurcation theory. Neural field equations of the form (1.6) also provide a framework for developing geometric-based approaches to vision [43].

In this paper, we exploit the product structure of the neural field equation (1.6) to analyze instabilities associated with nonhomogeneous solutions. More specifically, we consider two particular subclasses of solution, x-independent solutions for which

$$\tau \frac{\partial u(\theta,t)}{\partial t} = -u(\theta,t) + J_0 \int_{-\pi/2}^{\pi/2} w(\theta-\theta') F(u(\theta,t)) d\theta' \tag{1.7}$$

and θ-independent solutions for which

$$\tau \frac{\partial u(x,t)}{\partial t} = -u(x,t) + w_0 \int_{\mathbb{R}^d} J(|x-x'|) F(u(x',t)) dx', \tag{1.8}$$

with $J_0 = \int J(|x|)dx > 0$ and $w_0 = \int w(\theta)d\theta > 0$. The basic idea is that (1.7) may support a nontrivial θ-dependent solution around the ring, whose existence is independent of the weight distribution $J(x)$ (modulo the scale factor J_0), but whose stability depends crucially on the spatial degree(s) of freedom. Similarly, (1.8) may support a nontrivial x-dependent solution in $\mathbb{R}^d$, which is independent of the weight distribution $w(\theta)$ (modulo the scale factor w_0), but whose stability depends crucially on the orientation degree of freedom. For the sake of illustration, we will focus on two specific dynamical instabilities for a one-dimensional network ($d = 1$):

(I) A stationary bump solution $U(\theta)$ undergoing a Turing-like instability with respect to spatially periodic perturbations in the x-direction (sections 2 and 3).

(II) A traveling front solution $U(x - ct)$ with wave speed c undergoing a θ-dependent instability along the front (section 4).

In both cases, we use weakly nonlinear analysis to investigate the nature of these instabilities and compare our results with numerical simulations. We thus show how neural fields with an underlying product structure support a variety of nontrivial coherent states.

Finally, note that under some circumstances one could view a two-dimensional neural field as having a product structure according to the decomposition $\mathbb{R}^2 = \mathbb{R} \times \mathbb{R}$. However, this applies only when the weight distribution is separable. One example would be an excitatory Gaussian distribution for which $w(\mathbf{r}) \sim \mathrm{e}^{-(x^2+y^2)/\sigma^2}$. However, separability breaks down if one also includes inhibition via a Mexican hat function, or one has an anisotropic weight distribution $w(\mathbf{r}) \sim \mathrm{e}^{-(x^2+ay^2)/\sigma^2}$ expressed in polar coordinates. Another difference is that a feature space is typically compact. Nevertheless, there is an analogy between additional degrees of freedom in feature space destabilizing a one-dimensional front solution, and additional spatial degrees of freedom destabilizing a plane wave or other type of one-dimensional interface in a two-dimensional neural field [25, 26, 20].

2. Turing instability of a spatially uniform orientation bump.

2.1. Spatially uniform bumps. We begin our analysis of the product neural field (1.6) by considering an x-independent bump (stationary pulse) solution $u(x,\theta,t) \equiv U(\theta)$. Substituting into the reduced ring model (1.7) gives

$$U(\theta) = J_0 \int_{-\pi/2}^{\pi/2} w(\theta - \theta') F(U(\theta')) d\theta'.$$

Suppose that the local weight distribution consists of short-range excitation and longer-range inhibition. In particular, we take

$$w(\theta) = w_0 + w_2 \cos(2\theta) \tag{2.1}$$

with $w_2 > w_0 > 0$. Following the constructive approach of Amari [1], it is straightforward to show that for a Heaviside rate function $F(u) = H(u - \kappa)$, the ring model (1.7) can exhibit bistability, in which the zero stationary state solution $u(\theta) = 0$ for all θ is coexistent with a stationary bump solution (orientation tuning curve). Let Δ be the half-width of a bump solution $U(\theta)$ such that $U(\theta) > \kappa$ for $|\theta| < \Delta$ and $U(\theta) < \kappa$ for $|\theta| > \Delta$. Then

$$U(\theta) = J_0 \int_{-\Delta}^{\Delta} w(\theta - \theta') d\theta' = J_0 \left[W(\Delta + \theta) - W(\theta - \Delta) \right],$$

where

$$W(\theta) = \int_0^{\theta} w(y) dy = w_0 \theta + \frac{1}{2} w_2 \sin(2\theta) \tag{2.2}$$

for the given weight distribution (2.1). The width of a bump solution is then determined from the threshold condition $U(\Delta) = \kappa$:

$$\kappa = J_0 W(2\Delta). \tag{2.3}$$

Bump solutions can be obtained graphically by finding the intercept of the horizontal line $y = \kappa$ with the curve $y = W(2\Delta)$, as illustrated in Figure 3. It can also be shown that the bump is stable (modulo uniform shifts) if and only if $W'(2\Delta) < 0$, where the prime denotes differentiation with respect to the argument.

For the particular weight distribution given by (2.1), it is possible to analyze the existence and stability of bumps without recourse to Heaviside functions by exploiting the separability of the cosine function [32]. That is, the stationary bump solution satisfies

$$\begin{aligned} U(\theta) &= J_0 \int_{-\pi/2}^{\pi/2} (w_0 + w_2[\cos(2\theta)\cos(2\theta') + \sin(2\theta)\sin(2\theta')]) F(U(\theta')) d\theta' \\ &= A_0 + A_1 \cos(2\theta) + B_1 \sin(2\theta), \end{aligned}$$

where

$$A_0 = w_0 J_0 \int_{-\pi/2}^{\pi/2} F(U(\theta)) d\theta, \quad A_1 = w_2 J_0 \int_{-\pi/2}^{\pi/2} \cos(2\theta) F(U(\theta)) d\theta,$$

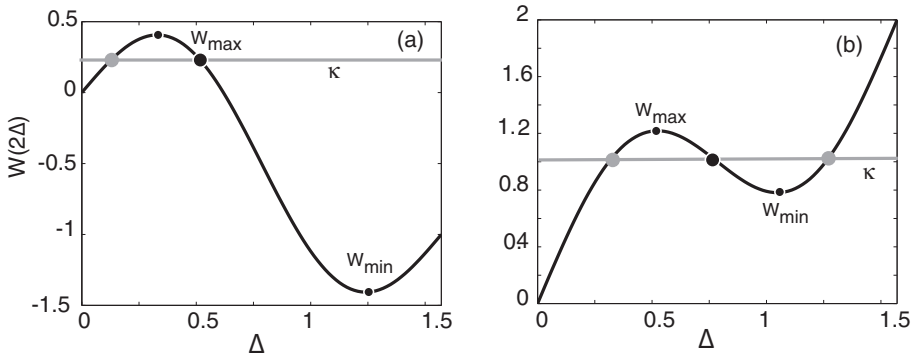

Figure 3. *Existence of bumps in the ring model. Plot of $W(2\Delta)$ as a function of Δ for $w_2 = 4/\pi$ and* (a) $w_0 = -1/\pi$, (b) $w_0 = 2/\pi$. *The intercepts of $W(2\Delta)$ with the horizontal line $y = \kappa$ determine the ξ-independent bump solutions. The left-hand figure has two bump solutions when $0 < \kappa < W_{\max}$, whereas the right-hand figure has three bump solutions when $W_{\min} < \kappa < W_{\max}$. Stable (unstable) bumps are indicated by black (gray) shaded circles.*

and

$$B_1 = w_2 J_0 \int_{-\pi/2}^{\pi/2} \sin(2\theta) F(U(\theta)) d\theta.$$

We look for an even bump solution so that $B_1 = 0$ and $U(\theta) = A_0 + A_1 \cos(2\theta)$. We can then numerically solve for A_0 and A_1 by imposing the self-consistency conditions

$$A_0 = w_0 J_0 \int_{-\pi/2}^{\pi/2} F(A_0 + A_1 \cos(2\theta)) d\theta \tag{2.4}$$

and

$$A_1 = w_2 J_0 \int_{-\pi/2}^{\pi/2} \cos(2\theta) F(A_0 + A_1 \cos(2\theta)) d\theta. \tag{2.5}$$

2.2. Linear stability analysis. The long-range weights $J(x)$ play no role with regards to the existence of x-independent bumps, other than the scale factor J_0. However, they play a major role in the stability of the bumps. Linear stability is investigated by linearizing the full neural field equation (1.6) about the bump solution. That is, set

$$u(x, \theta, t) = U(\theta) + v(x, \theta) e^{\lambda t}, \tag{2.6}$$

substitute into (1.6), and Taylor expand to first order in the perturbations $v(x, \theta)$. This yields the linear equation

$$(\lambda + 1) v(x, \theta) = \int_{\mathbb{R}} \int_{-\pi/2}^{\pi/2} w(\theta - \theta') F'(U(\theta')) J(x - x') v(x', \theta') d\theta' dx'. \tag{2.7}$$

Fourier transforming the linear equation with respect to x and using the convolution theorem gives

$$(\lambda + 1) \widetilde{V}(k, \theta) = \widetilde{J}(k) \int_{-\pi/2}^{\pi/2} w(\theta - \theta') F'(U(\theta')) \widetilde{V}(k, \theta') d\theta'. \tag{2.8}$$

Here

$$\widetilde{V}(k,\theta)=\int_{\mathbb{R}}\mathrm{e}^{ikx}v(x,\theta)dx,\quad v(x,\theta)=\int_{\mathbb{R}}\mathrm{e}^{-ikx}\widetilde{V}(k,\theta)\frac{dk}{2\pi}.$$

In the case of a Heaviside,

$$F'(U(\theta'))=H'(U(\theta')-\kappa)=\frac{\delta(\theta'-\Delta)}{|U'(\Delta)|}+\frac{\delta(\theta'+\Delta)}{|U'(-\Delta)|},$$

where Δ is the bump half-width, so that

$$(\lambda+1)\widetilde{V}(k,\theta)=\widetilde{J}(k)\left[\frac{w(\theta-\Delta)}{|U'(\Delta)|}\widetilde{V}(k,\Delta)+\frac{w(\theta+\Delta)}{|U'(-\Delta)|}\widetilde{V}(k,-\Delta)\right].$$

Setting $\theta=\pm\Delta$ then yields the 2×2 matrix equation

$$(\lambda+1)\begin{pmatrix}\widetilde{V}(k,\Delta)\\ \widetilde{V}(k,-\Delta)\end{pmatrix}=\frac{\widetilde{J}(k)}{|U'(\Delta)|}\begin{pmatrix}w(0) & w(2\Delta)\\ w(-2\Delta) & w(0)\end{pmatrix}\begin{pmatrix}\widetilde{V}(k,\Delta)\\ \widetilde{V}(k,-\Delta)\end{pmatrix},\tag{2.9}$$

with $|U'(-\Delta)|=|U'(\Delta)|$ and $w(-2\Delta)=w(2\Delta)$. Finally, noting that

$$|U'(\Delta)|=\widetilde{J}(0)[w(0)-w(2\Delta)],$$

we obtain two dispersion curves, $\lambda=\lambda_{\pm}(k)$ and

$$\lambda_{\pm}(k)=-1+\frac{\widetilde{J}(k)}{\widetilde{J}(0)}\frac{w(0)\pm w(2\Delta)}{w(0)-w(2\Delta)}.\tag{2.10}$$

The corresponding eigenvectors in real space take the form

$$v_{\pm}^{(k)}(x,\theta)=[w(\theta-\Delta)\pm w(\theta+\Delta)]\,\mathrm{e}^{ik(x-\phi)}+\text{c.c.},\tag{2.11}$$

where ϕ is an arbitrary phase due to the translation invariance of the system. For simplicity, we set $\phi=0$ and note that the phase of the growing mode will depend on initial conditions. It follows that $v_+(x,\theta)$ ($v_-(x,\theta)$) is an even (odd) function of θ. Setting $k=0$, we see that

$$\lambda_-(0)=0,\quad \lambda_+(0)=\frac{w(2\Delta)}{w(0)-w(2\Delta)},\tag{2.12}$$

and we recover Amari's standard stability condition that $w(2\Delta)<0$ [1]. The existence of a zero eigenvalue reflects homogeneity of the neural field equation with respect to θ. Thus, the x-independent bump is stable with respect to spatially uniform perturbations, which is one of the necessary conditions for a Turing instability. On the other hand, the bump can destabilize with respect to a spatially periodic perturbation. For nonzero k, we have

$$\lambda_-(k)=-1+\frac{\widetilde{J}(k)}{\widetilde{J}(0)}\tag{2.13}$$

and

$$\lambda_+(k) = -1 + \frac{\widetilde{J}(k)}{\widetilde{J}(0)} \frac{w(0) + w(2\Delta)}{w(0) - w(2\Delta)}. \tag{2.14}$$

In our analysis of spatially uniform bumps, we took $J_0 \equiv \widetilde{J}(0) > 0$ and required $W(2\Delta) < 0$ for stability. Therefore one possible scenario for a Turing instability is that at a critical value μ_c of some bifurcation parameter μ, we have $J_c = \max_{k\neq 0}\{\widetilde{J}(k)\} = \widetilde{J}(k_c) = J_0$ with $J_c < J_0$ for $\mu < \mu_c$ and $J_c > J_0$ for $\mu > \mu_c$. This will then result in the growth of the odd mode $v_-^{(k_c)}(x,\theta)$. It turns out that decomposing $J(x)$ into short-range connections and long-range, patchy horizontal connections exhibits such behavior. That is, following along similar lines to [33, 11], we consider a spatial weight distribution of the form

$$J(x) = \frac{1}{\sqrt{2\pi}} \left(\mathrm{e}^{-x^2/2\sigma_{\rm loc}^2} + \mu \cos(px) \mathrm{e}^{-x^2/2\sigma_{\rm hoz}^2} \right),$$

where $\sigma_{\rm loc}$ and $\sigma_{\rm hoz}$ specify the range of local and long-range connections, respectively, $2\pi/p$ is the period of patchy connections, and $\sigma_{\rm loc} < 2\pi/p < \sigma_{\rm hoz}$. To simplify calculations we can fix spatial scales so that $\sigma_{\rm loc} = 1$ and $\sigma_{\rm hoz} = \sigma$, so that

$$J(x) = \frac{1}{\sqrt{2\pi}} \left(\mathrm{e}^{-x^2/2} + \mu \cos(px) \mathrm{e}^{-x^2/2\sigma^2} \right). \tag{2.15}$$

The corresponding Fourier transform is

$$\widetilde{J}(k) = e^{-k^2/2} + \frac{\mu\sigma}{2} \left(e^{-(k-p)^2\sigma^2/2} + e^{-(k+p)^2\sigma^2/2} \right). \tag{2.16}$$

It is clear that $\widetilde{J}(k)$ has maxima at $k = 0, \pm p$ with $\widetilde{J}(p) = \widetilde{J}(0)$ at the critical parameter value $\mu = \mu_c$, where

$$\mu_c = \frac{1 - e^{-p^2/2}}{\sigma \left(\frac{1}{2} \left(1 + e^{-2p^2\sigma^2} \right) - e^{-p^2\sigma^2/2} \right)} > 0. \tag{2.17}$$

Hence, increasing μ from zero generates a pattern-forming instability at the critical wavenumber $k_c = p$, as illustrated in Figure 4. Thus the frequency of the growing pattern reflects the frequency of patchiness of horizontal connections.

In the case of a sigmoid rate function F with symmetric bump solution $U(\theta) = A_0 + A_1 \cos(2\theta)$, we have

$$(\lambda + 1)\widetilde{V}(k,\theta) = \widetilde{J}(k) \int_{-\pi/2}^{\pi/2} (w_0 + w_2[\cos(2\theta)\cos(2\theta') + \sin(2\theta)\sin(2\theta')]) \times F'(A_0 + A_1\cos(2\theta'))\widetilde{V}(k,\theta')d\theta'.$$

It follows that

$$\widetilde{V}(k,\theta) = V_0(k) + V_c(k)\cos(2\theta) + V_s \sin(2\theta), \tag{2.18}$$

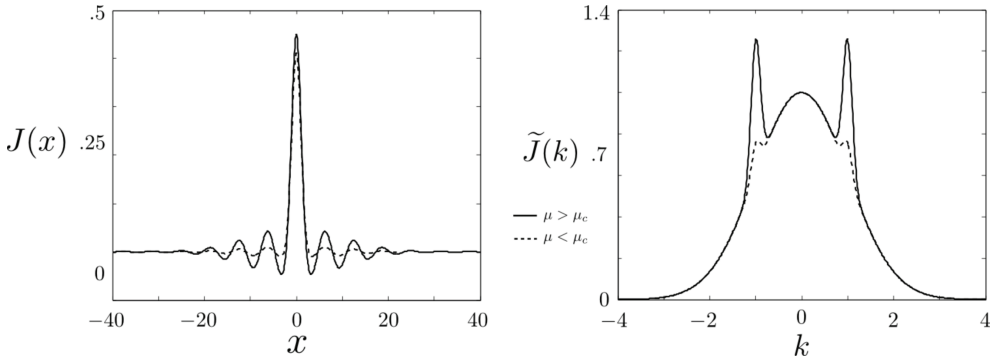

Figure 4. *Plot of $J(x)$ (left) and $\widetilde{J}(k)$ (right) for both $\mu > \mu_c$ (solid line) and $\mu < \mu_c$ (dashed line). Parameter values are $\sigma = 10$, $p = 1$, $\mu = 0.13$ for the solid line and $\mu = 0.03$ for the dotted line.*

with the k-dependent coefficients satisfying the self-consistency conditions

$$(\lambda+1)V_0(k) = w_0\widetilde{J}(k)\int_{-\pi/2}^{\pi/2} F'(A_0 + A_1\cos(2\theta'))] \times [V_0(k) + V_c(k)\cos(2\theta') + V_s\sin(2\theta')]d\theta',$$

$$(\lambda+1)V_c(k) = w_2\widetilde{J}(k)\int_{-\pi/2}^{\pi/2} \cos(2\theta')F'(A_0 + A_1\cos(2\theta'))] \times [V_0(k) + V_c(k)\cos(2\theta') + V_s\sin(2\theta')]d\theta',$$

and

$$(\lambda+1)V_s(k) = w_2\widetilde{J}(k)\int_{-\pi/2}^{\pi/2} \sin(2\theta')F(A_0 + A_1\cos(2\theta'))] \times [V_0(k) + V_c(k)\cos(2\theta') + V_s\sin(2\theta')]d\theta'.$$

Thus, for each k, we have a 3×3 eigenvalue problem for $\mathbf{V}(k) = (V_0(k), V_c(k), V_s(k))$:

$$(\lambda+1)\mathbf{V}(k) = \widetilde{J}(k)\begin{pmatrix} w_0\mathcal{K}_1(1) & w_0\mathcal{K}_1(\cos 2\theta) & w_0\mathcal{K}_1(\sin 2\theta) \\ w_2\mathcal{K}_1(\cos 2\theta) & w_2\mathcal{K}_1(\cos^2 2\theta) & w_2\mathcal{K}_1(\cos 2\theta\sin 2\theta) \\ w_2\mathcal{K}_1(\sin 2\theta) & w_2\mathcal{K}_1(\cos 2\theta\sin 2\theta) & w_2\mathcal{K}_1(\sin^2 2\theta) \end{pmatrix}\mathbf{V}(k),$$

where

$$\mathcal{K}_1(f(\theta)) = \int_{-\pi/2}^{\pi/2} f(\theta)F'(U(\theta))d\theta. \tag{2.19}$$

Integrating the condition (2.5) by parts gives

$$A_1 = A_1 w_2 J_0 \int_{-\pi/2}^{\pi/2} \sin^2(2\theta)F'(A_0 + A_1\cos(2\theta))d\theta. \tag{2.20}$$

Therefore, as long as $A_1 \neq 0$, we require

$$w_2 J_0 \mathcal{K}_1(\sin^2(2\theta)) = 1.$$

Since $U(\theta)$ is an even function of θ, we can set $\mathcal{K}_1(\cos 2\theta \sin 2\theta) = \mathcal{K}_1(\sin 2\theta) = 0$. Also $\mathcal{K}_1(\cos^2 2\theta) + \mathcal{K}(\sin^2 2\theta) = \mathcal{K}_1(1)$. Hence, we obtain the characteristic equation

$$(\lambda+1)\mathbf{V}(k) = \widetilde{J}(k) \begin{pmatrix} w_0\mathcal{K}_1(1) & w_0\mathcal{K}_1(\cos 2\theta) & 0 \\ w_2\mathcal{K}_1(\cos 2\theta) & w_2\mathcal{K}_1(\cos^2 2\theta) & 0 \\ 0 & 0 & \frac{1}{\widetilde{J}(0)} \end{pmatrix} \mathbf{V}(k). \tag{2.21}$$

Again, we will assume the odd mode grows, which occurs when $\widetilde{J}(k_c) > \widetilde{J}(0)$, so that the excited modes are of the form

$$v(x,\theta,\tau) = z(\tau)\sin(2\theta)e^{ik_c x} + \text{c.c.} \tag{2.22}$$

where $z(\tau)$ is a complex amplitude. Hence, in both the Heaviside and sigmoid cases, the excited modes take the form

$$v(x,\theta,\tau) = z(\tau)U'(\theta)e^{ik_c x} + \text{c.c.} \tag{2.23}$$

Note: The analysis can be generalized to functions of the form

$$J(x) = \frac{1}{\sqrt{2\pi}}\left(e^{-x^2/2} + \mu q(x) e^{-x^2/2\sigma^2}\right),$$

where $q(x)$ is an even $2\pi/p$-periodic function of the form

$$q(x) = \sum_{n=1}^{\infty} q_n \cos(pnx).$$

Then the Fourier transform is given by

$$\widetilde{J}(k) = e^{-k^2/2} + \frac{\mu\sigma}{2}\sum_{n=1}^{\infty} q_n \left(e^{-(k-np)^2\sigma^2/2} + e^{-(k+np)^2\sigma^2/2}\right)$$

so that for $\mu = \mu_c$

$$\max_n \widetilde{J}(np) = \widetilde{J}(0).$$

Then if $q_1 > q_n$ for all $n > 1$, we have the same result as before. In practice this can be assumed since the overall patchiness is $2\pi/p$-periodic and all other terms allow for small fluctuations in the profile. Therefore we can, without loss of generality, perform the analysis with the simpler weight function given by (2.15). As expected, some form of inhibition is required for a Turing instability to occur. Consider, for example, a weight function of the form

$$J(x) = \frac{1}{\sqrt{2\pi}}\left(e^{-x^2/2} + \mu(1+\cos(px))e^{-x^2/2\sigma^2}\right), \tag{2.24}$$

which is nonnegative for all x. The Fourier transform is then

$$\widetilde{J}(k) = e^{-k^2/2} + \frac{\mu}{2}\left(2e^{-k^2\sigma^2/2} + e^{-(k-p)^2\sigma^2/2} + e^{-(k+p)^2\sigma^2/2}\right) \tag{2.25}$$

so that there does not exist a $k \neq 0$ such that $\widetilde{J}(0) = \widetilde{J}(k)$ for any μ. Thus, both patchiness and inhibition is required for pattern formation in the given model.

2.3. Amplitude equation. We would now like to derive an amplitude equation for the growing mode causing instability in the fixed bump solution near the point of bifurcation, $\mu - \mu_c = \varepsilon\Delta\mu$. Near bifurcation, the unstable mode should grow like $e^{\Delta\mu\varepsilon t}$, so we introduce the slow time scale $\tau = \varepsilon t$. We can then write the solution to the neural field equation as a power series in ε,

$$u(x,\theta,\tau) = U_\mu(\theta) + \varepsilon^{1/2}u_1(x,\theta,\tau) + \varepsilon u_2(x,\theta,\tau) + \varepsilon^{3/2}u_3(x,\theta,\tau) + \mathcal{O}(\varepsilon^2). \tag{2.26}$$

Furthermore we must consider up to cubic terms in the expansion of the right-hand side of (1.6). Expanding the right-hand side of (1.6) about $U(\theta)$ and letting $u(x,\theta,\tau) \to u(x,\theta,\tau) - U(\theta)$, we have

$$\varepsilon u_\tau(x,\theta,\tau) = \mathcal{L}_\mu u(x,\theta,\tau) + \frac{1}{2}\mathcal{B}_\mu(u,u) + \frac{1}{6}\mathcal{C}_\mu(u,u,u) + \mathcal{O}(||u||^4), \tag{2.27}$$

where $\mathcal{L}_\mu, \mathcal{B}_\mu, \mathcal{C}_\mu : L^2(\Omega,\mathbb{R}) \to L^2(\Omega,\mathbb{R})$ are defined by

$$\mathcal{L}_\mu u(x,\theta,\tau) = -u(x,\theta,\tau) + \int_\Omega w(\theta-\theta')J_\mu(x-x')F'(U_\mu(\theta'))u(x',\theta',\tau)d\theta'dx', \tag{2.28}$$

$$\mathcal{B}_\mu(u,u) = \int_\Omega w(\theta-\theta')J_\mu(x-x')F''(U_\mu(\theta'))u(x',\theta',\tau)^2 d\theta'dx', \tag{2.29}$$

$$\mathcal{C}_\mu(u,u,u) = \int_\Omega w(\theta-\theta)J_\mu(x-x')F'''(U_\mu(\theta'))u(x',\theta',\tau)^3 d\theta'dx'. \tag{2.30}$$

Finally since these operators depend on μ we must also expand in powers of ε. We then obtain

$$\begin{aligned}
\mathcal{L}_\mu &= \mathcal{L}_{\mu_c} + \varepsilon\Delta\mu\frac{d}{d\mu}\mathcal{L}_\mu\big|_{\mu=\mu_c} + \mathcal{O}(\varepsilon^2) \equiv \mathcal{L}_{\mu_c} + \varepsilon\Delta\mu\mathcal{L}_1 + \mathcal{O}(\varepsilon^2),\\
\mathcal{B}_\mu &= \mathcal{B}_{\mu_c} + \mathcal{O}(\varepsilon),\\
\mathcal{C}_\mu &= \mathcal{C}_{\mu_c} + \mathcal{O}(\varepsilon).
\end{aligned}$$

Note that the higher order terms in the quadratic and cubic forms do not matter since we will be considering terms only up to $\mathcal{O}(\varepsilon^{3/2})$. Plugging the expansions into (2.27), we have

$$\begin{aligned}
\varepsilon^{3/2}\partial_\tau u_1 = {}& \varepsilon^{1/2}\mathcal{L}_{\mu_c}u_1 + \varepsilon\left[\mathcal{L}_{\mu_c}u_2 + \frac{1}{2}\mathcal{B}_{\mu_c}(u_1,u_1)\right]\\
&+ \varepsilon^{3/2}\left[\mathcal{L}_{\mu_c}u_3 + \Delta\mu\mathcal{L}_1u_1 + \mathcal{B}_{\mu_c}(u_1,u_2) + \frac{1}{6}\mathcal{C}_{\mu_c}(u_1,u_1,u_1)\right] + \mathcal{O}(\varepsilon^{5/2}),
\end{aligned}$$

which, by matching powers of ε, leads to the hierarchy of equations

$$\mathcal{L}_{\mu_c}u_1 = 0, \tag{2.31}$$

$$\mathcal{L}_{\mu_c}u_2 = -\frac{1}{2}\mathcal{B}_{\mu_c}(u_1,u_1), \tag{2.32}$$

$$\mathcal{L}_{\mu_c}u_3 = (\partial_\tau - \Delta\mu\mathcal{L}_1)u_1 - \mathcal{B}_{\mu_c}(u_1,u_2) - \frac{1}{6}\mathcal{C}_{\mu_c}(u_1,u_1,u_1). \tag{2.33}$$

We know from the linear analysis that

$$u_1(x,\theta,\tau) = z(\tau)v_1(x,\theta), \quad v_1(x,\theta) = \sin(2\theta)\cos(k_c x).$$

For concreteness, we fix the phase of the spatial part and take the amplitude $z(\tau)$ to be real. (The growing pattern is defined up to an arbitrary phase due to translation invariance with respect to x.) The Fredholm alternative theorem guarantees a solution to (2.32) and (2.33), provided the right-hand sides are orthogonal to the elements of the nullspace of $\mathcal{L}^*_{\mu_c}$ which is given by

$$\mathcal{L}^*_{\mu_c}u^* = -u^*(x,\theta) + F'(U_{\mu_c}(\theta))\int_\Omega w(\theta-\theta')J_{\mu_c}(x-x')u^*(x',\theta')d\theta' dx' \tag{2.34}$$

with respect to the inner product

$$\langle u, v\rangle = \frac{k_c}{\pi}\int_{-\pi/k_c}^{\pi/k_c}\int_{-\pi/2}^{\pi/2} u(x,\theta)v(x,\theta)d\theta dx. \tag{2.35}$$

(We choose this range of integration for x, since we will eventually be restricting the space of solutions to functions with wavenumber $k = k_c$.) Therefore an element of the nullspace of the adjoint operator satisfies

$$u^*(x,\theta) = F'(U_{\mu_c}(\theta))\int_\Omega w(\theta-\theta')J_{\mu_c}(x-x')u^*(x',\theta')d\theta' dx'.$$

This is equivalent to letting $u^*(x,\theta) = F'(U_{\mu_c}(\theta))v(x,\theta)$ with

$$\begin{aligned} v(x,\theta) &= \int_\Omega w(\theta-\theta')J_{\mu_c}(x-x')F'(U_{\mu_c}(\theta')v(x',\theta')d\theta' dx' \\ &= \mathcal{L}_{\mu_c}v(x,\theta) + v(x,\theta), \end{aligned}$$

which implies that if $v(x,\theta) \in \mathcal{N}(\mathcal{L}_{\mu_c})$, then $u^*(x,\theta) \in \mathcal{N}(\mathcal{L}^*_{\mu_c})$ with

$$u^*(x,\theta) = F'(U_{\mu_c}(\theta))\sin(2\theta)\cos(k_c x). \tag{2.36}$$

In order to solve (2.32) we observe that

$$\mathcal{B}_{\mu_c}(u_1,u_1) = z(\tau)^2\int_\Omega w(\theta-\theta')J_{\mu_c}(x-x')F''(U_{\mu_c}(\theta'))\sin^2(2\theta')\cos^2(k_c x')d\theta' dx'.$$

Since $F''(U_{\mu_c}(\theta'))$ and $\sin^2(2\theta)$ are even, then only the cosine terms are nonzero so that $\mathcal{B}_{\mu_c}(u_1,u_1)$ is an even function in θ, and since u^* is odd the Fredholm alternative is immediately satisfied. To solve for u_2, consider the equation

$$\begin{aligned} u_2(x,\theta,\tau) = &\int_\Omega w(\theta-\theta')J_{\mu_c}(x-x')F'(U_\mu(\theta'))u_2(x',\theta',\tau)d\theta' dx' \\ &+\frac{1}{2}z(\tau)^2\int_\Omega w(\theta-\theta')J_{\mu_c}(x-x')F''(U_{\mu_c}(\theta'))\sin^2(2\theta')\cos^2(k_c x')d\theta' dx'. \end{aligned}$$

It is easy to verify that the solution has the form $u_2(x,\theta,\tau) = z(\tau)^2 v_2(x,\theta)$ with

$$v_2(x,\theta) = \frac{1}{2}\left[A_0 + A_2\cos(2\theta) + (\widetilde{A}_0 + \widetilde{A}_2\cos(2\theta))\cos(2k_c x)\right], \tag{2.37}$$

where the coefficients satisfy the matrix equations

$$\begin{pmatrix} w_0\mathcal{K}(1) - J_0^{-1} & w_0\mathcal{K}(\cos(2\theta)) \\ w_2\mathcal{K}(\cos(2\theta)) & w_2\mathcal{K}(\cos^2(2\theta)) - J_0^{-1}\end{pmatrix}\begin{pmatrix} A_0 \\ A_2\end{pmatrix} = -\frac{1}{2}\begin{pmatrix} w_0\mathcal{K}_2(1) \\ w_2\mathcal{K}_2(\cos(2\theta))\end{pmatrix} \tag{2.38}$$

and

$$\begin{pmatrix} w_0\mathcal{K}(1) - \mathcal{I}(\cos(2k_c x))^{-1} & w_0\mathcal{K}(\cos(2\theta)) \\ w_2\mathcal{K}(\cos(2\theta)) & w_2\mathcal{K}(\cos^2(2\theta)) - \mathcal{I}(\cos(2k_c x))^{-1}\end{pmatrix}\begin{pmatrix} \widetilde{A}_0 \\ \widetilde{A}_2\end{pmatrix}$$
$$= -\frac{1}{2}\begin{pmatrix} w_0\mathcal{K}_2(1) \\ w_2\mathcal{K}_2(\cos(2\theta))\end{pmatrix}, \tag{2.39}$$

where $\mathcal{K}(f(\theta))$ is defined in (2.19) and

$$\mathcal{K}_2(f(\theta)) = \int_{-\pi/2}^{\pi/2} F''(U_{\mu_c}(\theta))\sin^2(2\theta) f(\theta)\,d\theta, \tag{2.40}$$

$$\mathcal{I}(f(x)) = \int_{-\infty}^{\infty} J_{\mu_c}(x) f(x)\,dx. \tag{2.41}$$

Note that we can add to u_2 a function of the form $h(x) = f(x)\sin(2\theta)$ and it will also be a solution. However, all odd modes will be projected out in the inner product since $\mathcal{B}_{\mu_c}(u_1,h)$ is an even function of θ when h is odd (due to the fact that u_1 is odd). Hence, since $u^*(x,\theta)$ is an odd function of θ we have $\langle \mathcal{B}_{\mu_c}(u_1,h), u^*\rangle = 0$. It follows that

$$\mathcal{B}_{\mu_c}(u_1,u_2) = \frac{1}{2}z(\tau)^3\sin(2\theta)(B_1\cos(k_c x) + B_2\cos(k_c x)\cos(2k_c x) + B_3\sin(k_c x)\sin(2k_c x)), \tag{2.42}$$

where

$$B_1 = w_2\mathcal{I}(\cos(k_c x))(A_0\mathcal{K}_2(1) + A_2\mathcal{K}_2(\cos(2\theta))),$$
$$B_2 = w_2\mathcal{I}(\cos(k_c x)\cos(2k_c x))(\widetilde{A}_0\mathcal{K}_2(1) + \widetilde{A}_2\mathcal{K}_2(\cos(2\theta))),$$
$$B_3 = w_2\mathcal{I}(\sin(k_c x)\sin(2k_c x))(\widetilde{A}_0\mathcal{K}_2(1) + \widetilde{A}_2\mathcal{K}_2(\cos(2\theta))).$$

Calculating the inner product of $\mathcal{B}_{\mu_c}(u_1,u_2)$ with $u^*(x,\theta)$ yields

$$\langle \mathcal{B}_{\mu_c}(u_1,u_2), F'(U_{\mu_c}(\theta))\sin(2\theta)\cos(k_c x)\rangle = \frac{1}{2}B\mathcal{K}(\sin^2(2\theta))z(\tau)^3, \tag{2.43}$$

where $B = B_1 + B_2/2 + B_3/2$.

The next step is to compute the cubic term. Noting that $F'''(U_{\mu_c}(\theta))\sin^3(2\theta)$ is an odd function, we have

$$\begin{aligned}\mathcal{C}_{\mu_c}(u_1,u_1,u_1) &= z(\tau)^3\int_\Omega w(\theta-\theta')J_{\mu_c}(x-x')F'''(U_{\mu_c}(\theta'))\\ &\qquad\times\sin^3(2\theta')\cos^3(k_cx)d\theta'dx'\\ &= z(\tau)^3\sin(2\theta)\big[C_1\cos(k_cx)+C_2\cos(3k_cx)\big],\end{aligned}\tag{2.44}$$

where, using the trigonometric identity $\cos^3(x)=(3\cos(x)+\cos(3x))/4$,

$$\begin{aligned}C_1&=\frac{3}{4}w_2\mathcal{I}(\cos(k_cx))\mathcal{K}_3(\sin(2\theta)),\\ C_2&=\frac{1}{4}w_2\mathcal{I}(\cos(3k_cx))\mathcal{K}_3(\sin(2\theta)),\end{aligned}$$

and

$$\mathcal{K}_3(f(\theta))=\int_{-\pi/2}^{\pi/2}F'''(U_{\mu_c}(\theta))\sin^3(2\theta')f(\theta)d\theta.\tag{2.45}$$

Computing the inner product of $\mathcal{C}_{\mu_c}(u_1,u_1,u_1)$ with $u^*(x,\theta)$, we have

$$\begin{aligned}&\langle\mathcal{C}_{\mu_c}(u_1,u_1,u_1),F'(U_{\mu_c}(\theta))\sin(2\theta)\cos(k_cx)\rangle\\ &=C_1\mathcal{K}(\sin^2(2\theta))z(\tau)^3\end{aligned}\tag{2.46}$$

since $\cos(k_cx)$ and $\cos(3k_cx)$ are orthogonal. Finally, we compute the operator $\mathcal{L}_1$. First, we note that the μ dependence in $\mathcal{L}_\mu$ appears in both the weight function $J_\mu(x)$ and in the bump solution $U_\mu(\theta)$. However, we note that

$$U_\mu\propto J_0=1+\mu\sigma e^{-p^2\sigma^2/2}$$

so that $dU_{\mu_c}/d\mu\ll1$. Therefore the main contribution comes from the μ dependence in $J_\mu(x)$. It then follows that

$$\begin{aligned}\mathcal{L}_1u(x,\theta,\tau)&=\int_\Omega w(\theta-\theta')\frac{\partial}{\partial\mu}J_\mu(x-x')F'(U_\mu(\theta'))u(x',\theta',\tau)d\theta'dx'\Big|_{\mu=\mu_c}\\ &\quad+\mathcal{O}\left(\sigma e^{-p^2\sigma^2/2}\right)\end{aligned}\tag{2.47}$$

and

$$\mathcal{L}_1u_1\approx\gamma z(\tau)\sin(2\theta)\cos(k_cx),\tag{2.48}$$

where

$$\gamma=w_2\mathcal{K}(\sin^2(2\theta))\partial_\mu\mathcal{I}(\cos(k_cx))\big|_{\mu=\mu_c}.\tag{2.49}$$

Alternatively, one could normalize the weight function so that J_0 is independent of μ, which makes $U(\theta)$ independent of μ, and the above is an exact equality.

Collecting our various calculations, we obtain the amplitude equation by taking the inner product of the right-hand side of (2.33) with $u^*(x,\theta)$ and setting it to zero:

$$\frac{dz}{d\tau} = \gamma\Delta\mu z + \beta z^3, \tag{2.50}$$

where γ is given as above and

$$\begin{aligned}\beta =& \frac{\langle \mathcal{B}_{\mu_c}(v_1(x,\theta),v_2(x,\theta)), F'(U_{\mu_c}(\theta))v_1(x,\theta)\rangle}{\langle v_1(x,\theta), F(U_{\mu_c}(\theta))v_1(x,\theta))\rangle} \\ &+ \frac{1}{6}\frac{\langle \mathcal{C}_{\mu_c}(v_1(x,\theta),v_1(x,\theta),v_1(x,\theta)), F(U_{\mu_c}(\theta))v_1(x,\theta)\rangle}{\langle v_1(x,\theta), F(U_{\mu_c}(\theta))v_1(x,\theta))\rangle}.\end{aligned} \tag{2.51}$$

Noting that

$$\langle \sin(2\theta)\cos(k_c x), F'(U_{\mu_c}(\theta))\sin(2\theta)\cos(k_c x)\rangle = \mathcal{K}(\sin^2(2\theta))$$

and using (2.43) and (2.46), we obtain $\beta = B/2 + C_1/6$.

In the appendix, we calculate the coefficients of the amplitude equation explicitly for a Heaviside rate function and show that $\gamma > 0$ and $\beta < 0$, and so the system undergoes a supercritical pitchfork bifurcation. That is, for $\mu < \mu_c$ the uniform bump solution is stable ($z = 0$ is the unique stable fixed point), and for $\mu > \mu_c$ the uniform bump solution destabilizes and a stable pattern forming solution emerges. The amplitude of the pattern is given by

$$z^* = \sqrt{\frac{-\gamma\Delta\mu}{\beta}}.$$

Sufficiently close to the bifurcation, we expect the resulting pattern to be given by

$$\begin{aligned}u(x,\theta) &= U(\theta) + Z^*\sin(2\theta)\cos(k_c x) \\ &= \widetilde{J}_0(2\Delta_{\mu_c}w_0 + w_2\sin(2\Delta_{\mu_c})\cos(2\theta)) + Z^*\sin(2\theta)\cos(k_c x) \\ &= \alpha_0 + \alpha(x)\cos(2\theta + \phi(x)),\end{aligned} \tag{2.52}$$

where $Z^* = \varepsilon^{1/2}z^*$ and Δ_{μ_c} is the width of the spatially uniform bump at the critical point. Moreover, $\alpha(x)$ and $\phi(x)$ are a space-dependent amplitude and phase, respectively, with

$$\begin{aligned}\alpha(x) &= \sqrt{\widetilde{J}_0^2 w_2^2\sin^2(2\Delta_{\mu_c}) + Z^{*2}\cos^2(k_c x)}, \\ \phi(x) &= \arctan\left(-\frac{Z^*\cos(k_c x)}{\widetilde{J}_0 w_2\sin(2\Delta_{\mu_c})}\right).\end{aligned}$$

We see that the instability causes both a periodic phase shift and an amplitude modulation of amplitude of the uniform bump solution. Moreover, there is a maximal phase shift in the bump solution so that only a certain range of orientations are represented by the network. The modulation of the bump amplitude indicates that certain orientations will have a greater representation in the network than others.

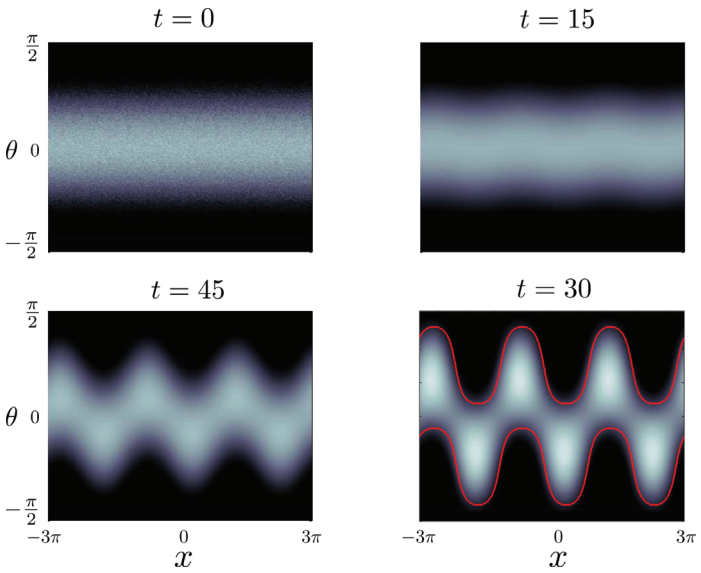

Figure 5. *Spatially periodic pattern emerging from a uniform orientation bump in the $x-\theta$ plane. Initial condition is the uniform bump solution plus noise. Parameter values: $w_0 = 0.25$, $w_2 = 1$, $\kappa = 0.5$, $\sigma = 10$ (for the exponential weight distribution), $p = 1$, and $\Delta\mu = 0.05$. A plot of the theoretical wave profile given by (2.52) is shown as a solid red curve in the last panel.*

3. Numerical results. We now simulate the Heaviside version of the neural field equation using a forward Euler method for the time derivative and trapezoidal rule for the convolutions. In Figure 5 we show the time evolution of the solution to the neural field equation with initial conditions given by the uniform bump solution, $U(\theta)$, plus random values assigned to each point on the grid, and the distance from the bifurcation point, $\Delta\mu = 0.05$. We see that the system indeed evolves to a pattern very similar to that found in the analysis. To ensure that this pattern was stable (modulo slow uniform shifts due to translation invariance), we ran the simulations repeatedly using final conditions as initial conditions in the next iteration plus noise. We found that for sufficiently small values of $\Delta\mu$ the analytical pattern is indeed stable. Plotting the stationary solution as a function of θ for various values of x, we see in Figure 6 that the bump is shifted in phase and modulated in amplitude as x changes, which agrees qualitatively with (2.52).

Increasing $\Delta\mu$ further, we found that a second pattern emerges of the form $\cos(2\theta + k_c x)$, up to an arbitrary phase, as shown in Figure 7 for $\Delta\mu = 0.2$. This indicates that the system undergoes a secondary bifurcation. The instability of the primary pattern is due to the growth of the even mode, $\cos(2\theta)\sin(k_c x)$. Equation (2.14) implies that $\lambda_+(k)$ can become positive for a sufficiently large value of μ. However, the value of μ at which λ_+ becomes positive is larger than the critical value of μ for the secondary bifurcation. Additionally, recall that the even and odd eigenfunctions are given by

$$v_{\pm}^{(k_c)}(x,\theta) = [w(\theta-\Delta) \pm w(\theta+\Delta)]\cos(k_c x + \phi_{\pm})$$

up to arbitrary phases $\phi_{\pm}$. The structure of the secondary pattern suggests that the phases of the even and odd eigenfunctions are correlated such that they are approximately 90° out

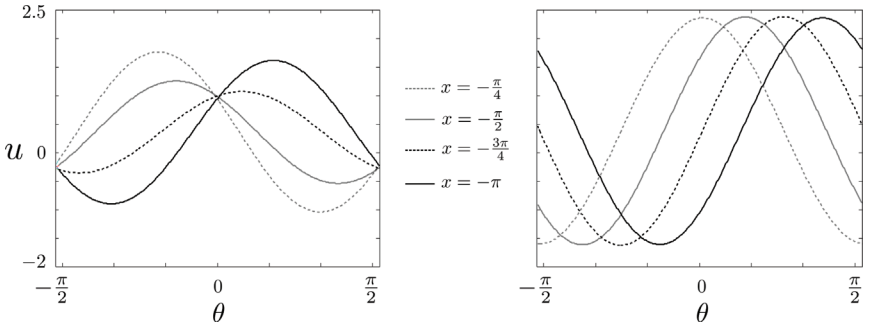

Figure 6. *Steady state solution as a function of θ and various values of x for primary bifurcation (left) and secondary bifurcation (right).*

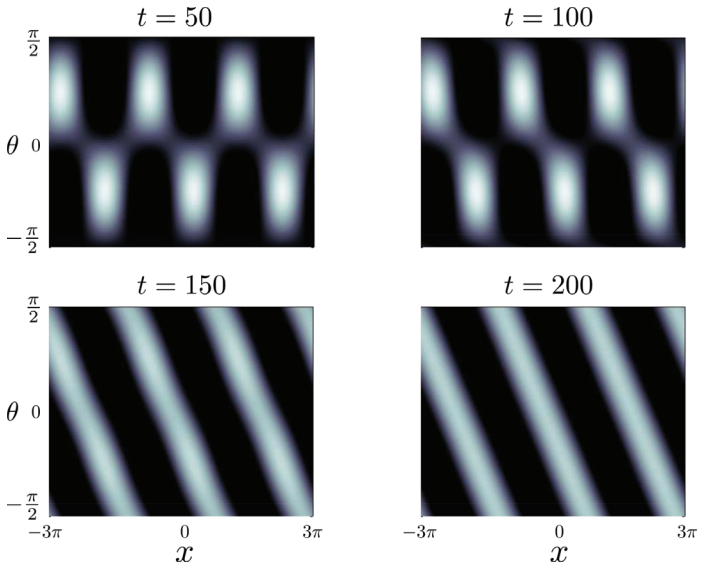

Figure 7. *Evolution of solution to the neural field equation in the $x-\theta$ plane following a secondary bifurcation. The initial condition is the primary pattern plus noise. Same parameter values as Figure 5, except that $\Delta\mu = 0.2$.*

of phase:

$$v_+^{(k_c)} = [w(\theta-\Delta)+w(\theta+\Delta)]\cos(k_c x) \propto \sin(2\theta)\cos(k_c x),$$
$$v_-^{(k_c)} = [w(\theta-\Delta)-w(\theta+\Delta)]\sin(k_c x) \propto (1+\alpha\cos(2\theta))\sin(k_c x).$$

Plotting the secondary pattern as a function of θ at various values of x, Figure 6 shows that the bump is shifted uniformly as x varies, while the amplitude of the bump remains approximately unchanged. Therefore, unlike the first pattern, all orientations are equally represented by the network and change periodically throughout space.

There is an important difference between the instabilities observed here and those arising from instabilities of a uniform solution $u(x,\theta) = U_0$. This is due to the fact that the latter preserves the equivariance of the product neural field equation (1.6) with respect to uniform shifts

$x \to x + a$ and $\theta \to \theta + b$. Thus a growing pattern has an arbitrary orientation phase. On the other hand, the x-independent bump solution $U(\theta)$ breaks the translation symmetry around the ring, and thus the growing patterns involve a specific orientation phase; that is, there is a separation between even modes $\cos(2\theta)$ and odd modes $\sin(2\theta)$. (An alternative mechanism for separating out odd and even modes is to have some anisotropy in the weights [13].)

4. Orientation-dependent instability of a traveling front.

4.1. Orientation-independent traveling fronts. As our second example of instabilities in product neural fields, we show how the product structure can destabilize a θ-independent traveling front. Suppose that $J(x)$ is a positive, monotonically decreasing function of $|x|$ such as a Gaussian or exponential function, and consider a traveling front solution of the form

$$u(x,\theta,t) = U(x-ct), \quad \lim_{\xi\to-\infty} U(\xi) = w_0 J_0 > \kappa, \quad \lim_{\xi\to\infty} U(\xi) = 0.$$

Setting $\xi = x - ct$ and substituting into (1.6) yields

$$-c\frac{\partial U}{\partial \xi} = -U + w_0 \int_{-\infty}^{\infty} d\xi' J(\xi - \xi') F(U(\xi')). \tag{4.1}$$

In the Heaviside case, $F(u) = H(u-\kappa)$, it is possible to construct an explicit front solution [1], and a continuation argument can be used to establish the existence of a front for a sigmoid function [23]. For simplicity, we will focus on the Heaviside rate function, since it is then possible to determine the stability of the front.

Exploiting translation invariance, we take the threshold crossing point to be at $\xi = 0$, that is, $U(\xi) > \kappa$ for $\xi < 0$ and $U(\xi) < \kappa$ for $\xi > 0$. Equation (4.1) becomes

$$-c\frac{\partial U}{\partial \xi} = -U + w_0 \int_{\xi}^{\infty} J(y)dy,$$

which can be rewritten as

$$\frac{d}{d\xi}\left[U(\xi)\mathrm{e}^{-\xi/c}\right] = -\frac{w_0}{c} e^{-\xi/c} K(\xi),$$

where

$$K(\xi) = \int_{\xi}^{\infty} J(y)dy.$$

Integrating from 0 to ∞ then gives the standard threshold condition

$$\kappa = \frac{w_0}{c}\int_0^{\infty} K(\xi)\mathrm{e}^{-\xi/c} d\xi. \tag{4.2}$$

In the case of an exponential weight distribution

$$J(x) = \frac{1}{2\sigma}\mathrm{e}^{-|x|/\sigma}, \tag{4.3}$$

one finds that for $0 < \kappa < w_0/2$ there is a unique front with speed

$$c = \frac{\sigma}{2\kappa}[w_0 - 2\kappa].$$

Although the existence of a front is independent of the orientation degree of freedom (modulo the scale factor w_0), the presence of the ring structure can affect the stability of the front. Linearizing the full product neural field equation (1.6) about the front solution by setting $F(u) = H(u - \kappa)$ and

$$u(x, \theta, t) = U(x - ct) + \varepsilon v(x - ct, \theta)\mathrm{e}^{\lambda t}$$

leads to the spectral problem

$$\begin{aligned} \lambda v(\xi, \theta) &= c\frac{\partial v}{\partial \xi} - v(\xi, \theta) + \int d\theta' w(\theta - \theta') \int d\xi' J(\xi - \xi')\frac{\delta(\xi')}{|U'(0)|} v(\xi', \theta') \\ &\equiv \mathcal{L}v(x, \theta). \end{aligned} \tag{4.4}$$

Taking Fourier components by setting $v(\xi, \theta) = \sum_n V_n(\xi)\mathrm{e}^{2in\theta}$ and letting

$$w(\theta) = \frac{1}{\pi}\left[w_0 + 2\sum_{n=1}^{\infty} w_{2n}\cos(2n\theta)\right] \tag{4.5}$$

gives

$$\lambda V_n(\xi) = c\frac{dV_n}{d\xi} - V_n(\xi) + \frac{w_{2n}}{|U'(0)|} J(\xi)V_n(0), \tag{4.6}$$

which can be rewritten as

$$\frac{d}{d\xi}\left[V_n(\xi)\mathrm{e}^{-(\lambda+1)\xi/c}\right] = -\frac{e^{-(\lambda+1)\xi/c} J(\xi)V_n(0)w_{2n}}{c|U'(0)|}. \tag{4.7}$$

Hence, we find that for $\lambda > -1$

$$V_n(\xi) = \frac{w_{2n}V_n(0)}{c|U'(0)|} \int_{\xi}^{\infty} \mathrm{e}^{-(\lambda+1)(y-\xi)/c} J(y)dy.$$

Finally, setting $\xi = 0$ generates the Evans function

$$\mathbb{E}(\lambda) = 1 - \frac{w_{2n}}{c|U'(0)|} \int_0^{\infty} \mathrm{e}^{-(\lambda+1)y/c} J(y)dy, \tag{4.8}$$

whose zeros determine the discrete spectrum. Set

$$\mathbb{H}(\lambda) = \int_0^{\infty} \mathrm{e}^{-(\lambda+1)y/c} J(y)dy. \tag{4.9}$$

The crucial point to observe is that

$$U'(\xi) = -\frac{w_0}{c} \int_{\xi}^{\infty} \mathrm{e}^{(\xi-y)/c} J(y)dy, \tag{4.10}$$

so that $c|U'(0)| = w_0\mathbb{H}(0)$. Hence the Evans function can be rewritten as

$$\mathbb{E}(\lambda) = 1 - \frac{w_{2n}}{w_0}\frac{\mathbb{H}(\lambda)}{\mathbb{H}(0)}. \tag{4.11}$$

The zeros of the Evans function then satisfy

$$\mathbb{H}(\lambda) = \frac{w_0}{w_{2n}}\mathbb{H}(0). \tag{4.12}$$

For positive, monotonically decreasing $J(x)$, we have that $\mathbb{H}(\lambda)$ is also monotonically decreasing. Therefore, for $w_{2n} < w_0$ the only λ that satisfy (4.12) are negative. Similarly for $w_{2n} > w_0$, λ must be positive, and for $w_{2n} = w_0$, $\lambda = 0$. Hence, there is a λ that becomes positive when $\max_n w_{2n}$ increases beyond w_0 and all other λ_n are negative. For the sake of illustration, we take $\max_n w_{2n} = w_2$. This would represent a synaptic weight distribution that is π-periodic with higher order terms to serve as small fluctuations in the overall profile. Therefore increasing w_2 will increase the strength of inhibition.

As an example, consider the case of the exponential weight function (4.3). We then obtain

$$\mathbb{H}(\lambda) = \frac{1}{2\sigma}\frac{c}{c/\sigma + \lambda + 1}$$

and

$$\mathbb{E}(\lambda) = 1 - \frac{w_{2n}}{w_0}\frac{c/\sigma + 1}{c/\sigma + \lambda + 1}. \tag{4.13}$$

It follows that zeros of the Evans function satisfy the equation

$$\lambda_n = \frac{w_{2n} - w_0}{w_0}(c/\sigma + 1). \tag{4.14}$$

In the trivial case that $w(\theta) = w_0$ then the only zero is $\lambda = 0$ and it is simple. Hence the traveling front is stable. However, for a θ-dependent weight distribution, there are a countable number of roots and the front will be unstable if

$$\max_n w_{2n} = w_{2n_c} > w_0$$

and the growing eigenfunction is given by

$$v(\xi, \theta) = \alpha \cos(2n_c\theta)\widehat{U}'(\xi), \tag{4.15}$$

where α is arbitrary and

$$\widehat{U}'(\xi) = \int_\xi^\infty e^{-(\lambda_n+1)(y-\xi)/c} J(y)dy. \tag{4.16}$$

We see that, up to a constant multiple, $\widehat{U}'(\xi)$ has the same form as $U'(\xi)$ by letting $c \to c/(\lambda_n + 1)$. Since the derivative of a traveling front is a pulse, it is clear that the growing

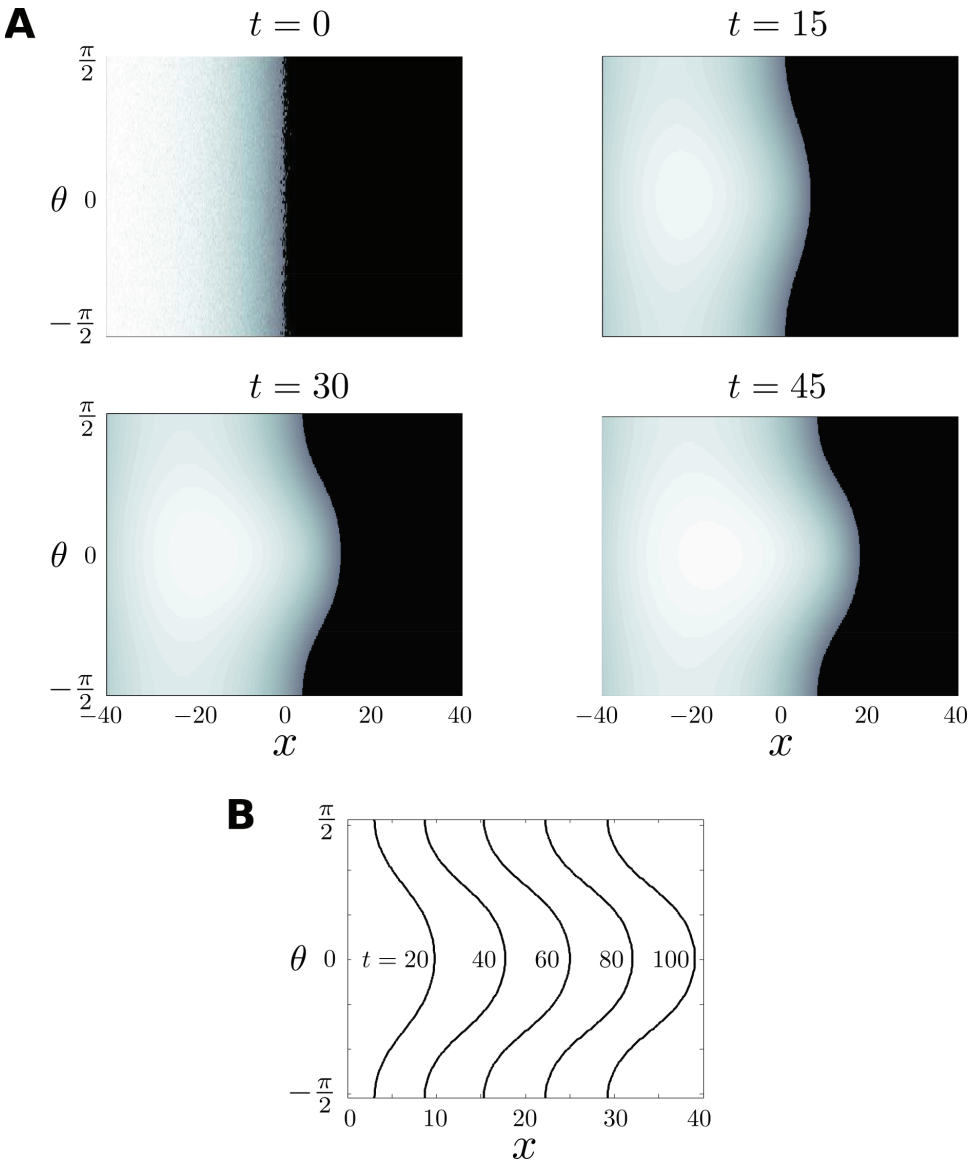

Figure 8. (A) *Orientation bump emerging from a traveling front. Initial condition taken to be the uniform traveling front solution plus noise. Only the region where $u > \kappa$ is plotted for clarity. Parameter values: $w_0 = 0.5$, $w_2 = 0.51$, $\kappa = 0.24$, $\sigma = 10$ (for the exponential weight distribution).* (B) *Successive snapshots of the front indicating that the front converges to a stable wave, consistent with our weakly nonlinear analysis.*

mode causes the appearance of a bump in a localized region in space and appears in the vicinity of the wave front. This is illustrated in Figure 8 for $n_c = 1$, which shows that as time progresses an orientation bump forms at the location of the wavefront. Snapshots of the front are shown in Figure 9.

A word of caution is necessary. We have assumed that the spatial weight distribution $J(x)$ is purely excitatory in order to obtain traveling fronts in $\mathbb{R}$. Typically, such a scenario mimics

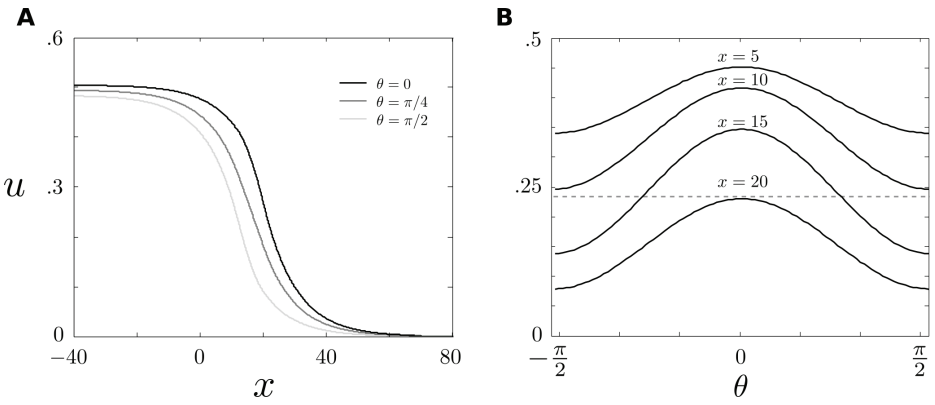

Figure 9. *Traveling wave solution at various values of* θ (A) *and* x (B) *at* $t = 45$. *Dashed line indicates* $u = \kappa$.

the pharmacological removal of inhibition in cortical slice experiments [38, 39]. On the other hand, we require inhibition in the orientation weight distribution $w(\theta)$, in order to have a bump instability. Another simplification that we have made is to ignore the effects of adaptation, which tend to hyperpolarize the trailing edge of the front, resulting in a propagating pulse instead. Hence, the above example is illustrative in nature and is not meant to be a realistic model of cortical waves [10]. Having said this, the precise dependence of excitation and inhibition on spatial and feature-based labels is still not clear and is likely to vary depending on stimulus conditions. Moreover, fronts rather than pulses do occur in the case of binocular rivalry waves [53, 14, 52].

4.2. Amplitude and phase equations. We now derive both an amplitude and phase equation for the growing spatially localized bump near the point of bifurcation $w_{2n_c} - w_0 = \varepsilon\Delta\mu$. Since the exponential weight function is not differentiable at $x = 0$, we assume that there exists a smooth weight function (or at least C^3) that has the property that yields the conditions, $\lambda_{n_c} \geq 0$ when $w_{2n_c} \geq w_0$ and $\lambda_n < 0$ for all $n \neq 0, n_c$.

Similar to section 2.3, we introduce the slow time scale $\tau = \varepsilon t$ and write the solution to the neural field equation as a power series in ε,

$$u(x,\theta,t,\tau) \equiv u(\xi - \phi(\tau),\theta,\tau) = U_0(\xi-\phi(\tau)) + \varepsilon^{1/2}u_1(\xi-\phi(\tau),\theta,\tau) + \varepsilon u_2(\xi-\phi(\tau),\theta,\tau) + \varepsilon^{3/2}u_3(\xi-\phi(\tau),\theta,\tau) + \mathcal{O}(\varepsilon^2),$$

where U_0 is the traveling front solution found in section 4.1, $\xi = x - ct$, and $\phi(\tau)$ is the phase advancement/retardation of the front. This form is motivated by analysis of fronts in stochastic neural fields where it is assumed that stochasticity causes diffusion in the position of the front and overall higher order fluctuations in the profile [15, 52]. Typically only terms up to $\mathcal{O}(\varepsilon^{1/2})$ are considered when finding an effective diffusion equation for the position of the front. However, we require higher order terms to show that the growth of the instability will eventually saturate.

Linearizing the right-hand side of the neural field equation about $U_0(\xi - \phi(\tau))$, we have

$$\varepsilon u_\tau = \mathcal{L}_\mu \overline{u} + \frac{1}{2}\mathcal{B}_\mu(\overline{u},\overline{u}) + \frac{1}{6}\mathcal{C}_\mu(\overline{u},\overline{u},\overline{u}) + \mathcal{O}(||\overline{u}||^4), \tag{4.17}$$

where $\overline{u} = u - U_0(\xi - \phi(\tau))$ and $\mathcal{L}_\mu, \mathcal{B}_\mu, \mathcal{C}_\mu : L^2(\Omega, \mathbb{R}) \to L^2(\Omega, \mathbb{R})$ are defined by

$$\begin{aligned}\mathcal{L}_\mu u = & c\partial_\xi u(\xi - \phi(\tau), \theta, \tau) - u(\xi - \phi(\tau), \theta, \tau) \\ & + \int_\Omega w(\theta - \theta')J(\xi - \xi')F'(U_0(\xi' - \phi(\tau)))u(\xi' - \phi(\tau), \theta', \tau)d\theta' d\xi', \end{aligned} \tag{4.18a}$$

$$\mathcal{B}_\mu(u, u) = \int_\Omega w(\theta - \theta')J(\xi - \xi')F''(U_0(\xi' - \phi(\tau)))u(\xi' - \phi(\tau), \theta', \tau)^2 d\theta' d\xi', \tag{4.18b}$$

$$\mathcal{C}_\mu(u, u, u) = \int_\Omega w(\theta - \theta')J(\xi - \xi')F'''(U_0(\xi' - \phi(\tau)))u(\xi' - \phi(\tau), \theta', \tau)^3 d\theta' d\xi'. \tag{4.18c}$$

Furthermore, we again expand $\mathcal{L}_\mu$ as

$$\mathcal{L}_\mu = \mathcal{L}_{\mu_c} + \varepsilon\Delta\mu\partial_\mu\mathcal{L}\big|_{\mu=w_0} \equiv \mathcal{L}_{\mu_c} + \varepsilon\Delta\mu\mathcal{L}_1, \tag{4.19}$$

where

$$\mathcal{L}_1 = \frac{2}{\pi}\int_\Omega \cos(2n_c(\theta - \theta'))J(\xi - \xi')F'(U_0(\xi'))u(\xi', \theta', \tau)d\theta' d\xi'. \tag{4.20}$$

Substituting these into the neural field equation and shifting $\xi - \phi(\tau) \to \xi$ yields the hierarchy of equations

$$\mathcal{L}_{\mu_c} u_1 = 0, \tag{4.21a}$$

$$\mathcal{L}_{\mu_c} u_2 = -\phi'(\tau)U_0' - \frac{1}{2}\mathcal{B}_{\mu_c}(u_1, u_1), \tag{4.21b}$$

$$\mathcal{L}_{\mu_c} u_3 = (\partial_\tau - \Delta\mu\mathcal{L}_1)u_1 - \phi'(\tau)\partial_\xi u_1 - \mathcal{B}_{\mu_c}(u_1, u_2) - \frac{1}{6}\mathcal{C}_{\mu_c}(u_1, u_1, u_1). \tag{4.21c}$$

Note that we are allowed to perform this shift since all terms include $\xi - \phi(\tau)$ and the system is translation invariant. Equation (4.21a) is immediately satisfied by the solution

$$u_1(\xi, \theta, \tau) = z(\tau)\cos(2n_c\theta)U_0'(\xi). \tag{4.22}$$

Solvability of (4.21b) and (4.21) is guaranteed if the right-hand sides are orthogonal to the elements of the nullspace of $\mathcal{L}^*_{\mu_c}$, which is given by

$$\begin{aligned}\mathcal{L}^*_{\mu_c} u^* = & -c\partial_\xi u^*(\xi, \theta) - u^*(\xi, \theta) \\ & + F'(U_0(\xi))\int_\Omega w(\theta - \theta')J(\xi - \xi')u^*(\xi', \theta')d\theta' d\xi' \end{aligned} \tag{4.23}$$

with respect to the inner product

$$\langle u, v\rangle = \frac{2}{\pi}\int_\Omega u(\xi, \theta)v(\xi, \theta)d\theta d\xi. \tag{4.24}$$

Consider a trial solution of the form

$$u^*(\xi, \theta) = \mu_p(\xi)\cos(2p\theta)$$

so that

$$c\partial_\xi \mu_p(\xi) + \mu_p(\xi) = w_{2p} F'(U_0(\xi)) \int_{-\infty}^{\infty} J(\xi - \xi')\mu_p(\xi')d\xi'.$$

We thus require

$$\mu_p(\xi) = \frac{w_{2p}}{c} \int_{-\infty}^{\xi} e^{(\xi'-\xi)/c} F'(U_0(\xi')) \int_{-\infty}^{\infty} J(\xi' - \xi'')\mu_p(\xi'')d\xi''d\xi'. \tag{4.25}$$

Setting $F(u) = H(u - \kappa)$, we have (see the appendix) $F'(U_0(\xi)) = \delta(U_0(\xi) - \kappa) = \frac{1}{|U_0'(0)|}\delta(\xi)$, so it is clear that

$$\mu_p(\xi) = AH(\xi)e^{-\xi/c}, \tag{4.26}$$

with (4.25) reducing to the condition

$$1 = \frac{w_{2p}}{c|U'(0)|} \int_0^{\infty} \mathrm{e}^{-y/c} J(y)dy. \tag{4.27}$$

Using the identity (4.10), we see that a null solution of the adjoint operator is given by

$$v_p(\xi) = H(\xi)\mathrm{e}^{-\xi/c} \cos(2p\theta),$$

provided that $w_{2p} = w_0$. A similar result holds by replacing $\cos(2p\theta)$ by 1 and $\sin(2p\theta)$. Hence, at the bifurcation point, we have a three-dimensional nullspace spanned by

$$\{H(\xi)e^{-\xi/c}, H(\xi)e^{-\xi/c}\cos(2n_c\theta), H(\xi)e^{-\xi/c}\sin(2n_c\theta)\} \in \mathcal{N}(\mathcal{L}^*).$$

For calculation purposes, we will use $u^*(\xi, \theta) = H(\xi)e^{-\xi/c}\cos(2n_c\theta)$. Computing $\mathcal{B}_{\mu_c}(u_1, u_1)$, we obtain

$$\mathcal{B}_{\mu_c}(u_1, u_1) = \frac{1}{2} z(\tau)^2 (w_0 + w_{4n_c}\cos(4n_c\theta))I_1(\xi) \tag{4.28}$$

with

$$I_1(\xi) = \int_{-\infty}^{\infty} J(\xi - \xi')F''(U_0(\xi'))U_0'(\xi')^2 d\xi'. \tag{4.29}$$

It immediately follows that the $\cos(2n_c\theta)$ and $\sin(2n_c\theta)$ terms in the adjoint nullspace are orthogonal to $\mathcal{B}_{\mu_c}(u_1, u_1)$ as well as U_0'. Thus, in order to solve for $\phi'(\tau)$ we require that

$$\langle H(\xi)e^{-\xi/c}, -\phi'(\tau)U_0' - \mathcal{B}_{\mu_c}(u_1, u_1)/2\rangle = 0,$$

which implies

$$\begin{aligned}\phi'(\tau) &= -\frac{1}{2}\frac{\langle H(\xi)e^{-\xi/c}, \mathcal{B}_{\mu_c}(u_1, u_1)\rangle}{\langle U_0'(\xi), H(\xi)e^{-\xi/c}\rangle} \\ &= -\frac{1}{4} z(\tau)^2 w_0 \frac{\int_0^{\infty} e^{-\xi/c} I_1(\xi)d\xi}{\int_0^{\infty} e^{-\xi/c} U_0'(\xi)d\xi}\end{aligned} \tag{4.30}$$

since $\int_0^\infty e^{-\xi/c}U_0'(\xi)d\xi \neq 0$. In the case of a Heaviside firing rate we have

$$\begin{aligned} I_1(\xi) &= -\frac{1}{|U_0'(0)|}\partial_{\xi'}\left(J(\xi-\xi')U_0'(\xi')\right)\Big|_{\xi'=0} \\ &= -\frac{1}{|U_0'(0)|}\left[J(\xi)U_0''(0) - J'(\xi)U_0'(0)\right], \end{aligned}$$

where we have used the identity $F''(U_0(\xi)) = \delta'(U_0(\xi)-\kappa)$ and [24]

$$\int \delta'(f(x))g(x)dx = -\int \delta(f(x))\frac{d}{dx}\left[\frac{g(x)}{f'(x)}\right]dx.$$

Integrating by parts and noting that $U_0''(0) = (U_0'(0) + w_0J(0))/c$ and $U_0'(0) = -w_0\mathbb{H}(0)/c$, we have

$$\int_0^\infty e^{-\xi/c}I_1(\xi)d\xi = 0,$$

so that $\phi'(\tau)$ and $\phi(\tau) = \phi_0$ a constant.

Now, solving for u_2 we obtain

$$\begin{aligned} &c\partial_\xi u_2 - u_2 + \int_\Omega w(\theta-\theta')J(\xi-\xi')F'(U_0'(\xi'))u_2(\xi',\theta',\tau)d\theta'd\xi' \\ &= -\frac{1}{4}z(\tau)^2(w_0 + w_{4n_c}\cos(4n_c\theta))I_1(\xi), \end{aligned}$$

which has the solution

$$u_2(\xi,\theta,\tau) = -\frac{1}{4c}z(\tau)^2(w_0 + w_{4n_c}\cos(4n_c\theta))A(\xi), \tag{4.31}$$

where

$$A(\xi) = \int_0^\xi e^{(\xi-\xi')/c}I_1(\xi')d\xi'. \tag{4.32}$$

Note that there are other solutions; however, we are at liberty to use functions for which $u_2(0,\theta,\tau) = 0$ so that we have the simple form above. Therefore,

$$\begin{aligned} \mathcal{B}_{\mu_c}(u_1,u_2) =& \frac{1}{4c|U_0'(0)|}z(\tau)^3\int_{-\pi/2}^{\pi/2} w(\theta-\theta')\cos(2n_c\theta')(w_0 + w_{4n_c}\cos(4n_c\theta'))d\theta' \\ &\times \partial_{\xi'}(J(\xi-\xi')A(\xi'))\big|_{\xi'=0} \\ =& -\frac{J(0)U_0''(0)}{4c|U'(0)|^2}z(\tau)^2b(\theta)J(\xi), \end{aligned} \tag{4.33}$$

where

$$b(\theta) = w_{2n_c}\left(w_0 + \frac{1}{2}w_{4n_c}\right)\cos(2n_c\theta) + \frac{w_{4n_c}w_{6n_c}}{2}\cos(6n_c\theta). \tag{4.34}$$

We have used the fact that

$$A'(0) = I_1(0) = -\frac{J(0)U_0''(0)}{|U_0'(0)|} \tag{4.35}$$

since $J'(0) = 0$ ($J(\xi)$ is a smooth even function). Taking the inner product with $u^*(\xi,\theta)$, we define

$$\begin{aligned} B_1 &= \langle \mathcal{B}_{\mu_c}(u_1,u_2), H(\xi)e^{-\xi/c}\cos(2n_c\theta)\rangle \\ &= -\frac{J(0)U_0''(0)w_0(2w_0+w_{4n_c})\mathbb{H}(0)}{8c|U_0'(0)|^2}. \end{aligned} \tag{4.36}$$

Next, calculating the cubic term yields

$$\begin{aligned} \mathcal{C}_{\mu_c}(u_1,u_1,u_1) &= \frac{1}{4}z(\tau)^3\left(3w_{2n_c}\cos(2n_c\theta)+w_{6n_c}\cos(6n_c\theta)\right) \\ &\quad\times\frac{1}{|U_0'(0)|}\partial_{\xi'}\left(\frac{1}{U_0'(\xi)}\partial_{\xi'}\left(J(\xi-\xi')U_0'(\xi')^2\right)\right)\Big|_{\xi'=0} \\ &\equiv \frac{1}{4|U_0'(0)|}z(\tau)^3\left(3w_{2n_c}\cos(2n_c\theta)+w_{6n_c}\cos(6n_c\theta)\right)I_2(\xi), \end{aligned}$$

where

$$I_2(\xi) = U_0'(0)J''(\xi) - 3U_0''(0)J'(\xi) + 2U_0'''(0)J(\xi), \tag{4.37}$$

and we have used the identity $F'''(U_0(\xi)) = \delta''(U_0(\xi)-\kappa)$ with [24]

$$\int \delta''(f(x))g(x)dx = \int \delta(f(x))\frac{d}{dx}\left[\frac{1}{f'(x)}\frac{d}{dx}\left[\frac{g(x)}{f'(x)}\right]\right]dx.$$

Noting that

$$U'''(0) = \frac{U''(0)+w_0J'(0)}{c} = \frac{U''(0)}{c},$$

since $J'(0)=0$, integrating by parts yields

$$\int_0^\infty e^{-\xi/c}I_2(\xi) = \frac{3J(0)w_0(cJ(0)-\mathbb{H}(0))}{c^2},$$

and therefore taking the inner product yields

$$C_1 = \langle \mathcal{C}_{\mu_c}(u_1,u_1,u_1), H(\xi)e^{-\xi/c}\cos(2n_c\theta)\rangle = \frac{9J(0)w_0(cJ(0)-\mathbb{H}(0))}{4c\mathbb{H}(0)}. \tag{4.38}$$

We then define

$$\alpha = \int_0^\infty e^{-\xi/c}U_0'(\xi)d\xi, \tag{4.39}$$

which is negative since $U_0'(\xi) < 0$ for all ξ ($U_0(\xi)$ is monotonically decreasing), and

$$\beta = \frac{\frac{1}{6}C_1 + B_1}{\langle U_0'(\xi)\cos(2n_c\theta), H(\xi)e^{-\xi/c}\cos(2n_c\theta)\rangle} = \frac{J(0)(w_0 - w_{4n_c})(cJ(0) - \mathbb{H}(0))}{8\alpha c\mathbb{H}(0)}. \tag{4.40}$$

Since $w_{4n_c} < w_0$, $\alpha < 0$ and

$$\mathbb{H}(0) = \int_0^\infty e^{-\xi/c}J(\xi)d\xi < J(0)\int_0^\infty e^{-\xi/c} = cJ(0), \tag{4.41}$$

we have that $\beta < 0$.

Finally, it is easy to see that

$$\mathcal{L}_1 u_1 = -z(\tau)\cos(n_c\theta)J(\xi) \tag{4.42}$$

and

$$\frac{\langle H(\xi)e^{-\xi/c}\cos(2n_c\theta), \mathcal{L}_1 u_1\rangle}{\langle H(\xi)e^{-\xi/c}\cos(2n_c\theta), \cos(2n_c\theta)U_0'(\xi)\rangle} = -\frac{\mathbb{H}(0)}{\alpha}z(\tau) \equiv \gamma z(\tau). \tag{4.43}$$

Thus, taking the inner product of (4.21b) with $u^*(x,\theta,\tau)$ and solving for $z'(\tau)$, we obtain

$$\frac{dz}{d\tau} = \gamma\Delta\mu z + \beta z^3 \tag{4.44}$$

with $\gamma > 0$ and $\beta < 0$. Hence, the amplitude undergoes a pitchfork bifurcation as w_{2n_c} increases above w_0 and the traveling bump solution is stable for $w_{2n_c} > w_0$.

5. Discussion. To summarize, we have shown that classical orientation bumps in S^1 and traveling front solutions in $\mathbb{R}$ can destabilize when considering a neural field equation on the product space $\mathbb{R} \times S^1$; the latter reflects the hypercolumnar structure of cortex. Although these solutions are stable when considering networks that are responsive to either orientation θ or position x, but not both, we found that incorporating both features as a product structure destabilizes these solutions, yielding more exotic dynamics. First, we showed how spatially periodic patterns emerge from an orientation bump when the strength of patchiness in horizontal connections exceeds some critical value. Second, we showed how a propagating orientation bump emerges at the front of a traveling wave when the strength of inhibition in orientation preference exceeds some critical value. These instabilities differ from previous studies of product neural fields, which focused on destabilization of a uniform state in a two-dimensional version of the model, that is, $\mathbb{R}^2 \times S^1$ [13].

One immediate extension of our work would be to consider instabilities of nonuniform states in the case of two-spatial dimensions. For example, one could consider two-dimensional stripe and hexagonal patterns emerging from a spatially uniform orientation bump, and bump instabilities emerging at the boundaries of spatial target patterns. The former could then be compared to the hallucinatory patterns bifurcating from a uniform state. Another extension would be to incorporate additional stimulus features such as spatial frequency. Assuming that iso-orientation and iso-frequency contours intersect approximately orthogonal to each other at pinwheels, one could use an orthogonal coordinate system and model the neural field on

$\mathbb{R}^2 \times S^2$, where S^2 is the surface of a sphere [8]. Yet another future direction would be to explore how the product structure destabilizes other types of solutions in standard neural field equations, such as traveling pulses and oscillatory patterns. Finally, it would be interesting to incorporate product structures into stochastic neural fields [15, 52] and to consider possible correlations between different degrees of freedom. In addition to the mathematical aspects of product neural fields, there are also potential neurobiological applications. One example is to develop a neural field model of binocular rivalry waves that explicitly incorporates the orientation preferences of neurons. In our previous work, we focused on an effective one-dimensional model that only took into account the activity of neurons that respond maximally to a given monocular stimulus [14, 52]. However, this is not sufficient for modeling rivalry waves associated with more complex annular stimuli, for example [53].

Appendix A. Explicit results for a Heaviside firing rate function. The coefficients in the amplitude equation can be numerically calculated for any arbitrary firing rate function since everything is known. However, one can carry out explicit calculations using a Heaviside firing rate function $F(u) = H(u - \kappa)$ and the weight function given by (2.15). In this case we have that the μ-dependent fixed bump solution is given by

$$U_{\mu_c}(\theta) = \widetilde{J}_{\mu_c}(0)\left(2\Delta_{\mu_c} w_0 + w_2 \sin(2\Delta_{\mu_c})\cos(2\theta)\right),$$

so that

$$U'_{\mu_c}(\Delta_{\mu_c}) = -2w_2 \widetilde{J}_{\mu_c}(0)\sin(2\Delta_{\mu_c})\sin(2\theta).$$

The functionals used in the previous section are given explicitly as

$$\mathcal{K}_1(f(\theta)) = \int_{-\pi/2}^{\pi/2} \left[\frac{\delta(\theta+\Delta_{\mu_c}) + \delta(\theta-\Delta_{\mu_c})}{\Gamma}\right] f(\theta)d\theta,$$

$$\mathcal{K}_2(f(\theta)) = -\int_{-\pi/2}^{\pi/2} \left[\frac{\delta(\theta+\Delta_{\mu_c}) + \delta(\theta-\Delta_{\mu_c})}{\Gamma}\right] \partial_\theta \left(\frac{f(\theta)\sin^2(2\theta)}{U'_{\mu_c}(\theta)}\right) d\theta,$$

$$\mathcal{K}_3(f(\theta)) = \int_{-\pi/2}^{\pi/2} \left[\frac{\delta(\theta+\Delta_{\mu_c}) + \delta(\theta-\Delta_{\mu_c})}{\Gamma}\right] \partial_\theta \left(\frac{1}{U'_{\mu_c}(\theta)}\partial_\theta \left(\frac{f(\theta)\sin^3(2\theta)}{U'_{\mu_c}(\theta)}\right)\right) d\theta,$$

$$\mathcal{I}(f(x)) = \frac{1}{\sqrt{2\pi}} \int_{-\infty}^{\infty} \left(e^{-x^2/2} + \mu e^{-x^2/2\sigma^2}\cos(px)\right) f(x)dx,$$

and we have defined

$$\Gamma = |U'_\mu(\Delta_{\mu_c})|.$$

Note that we have used the fact that for a Heaviside firing rate

$$F'(U_{\mu_c}(\xi)) = \delta(U_{\mu_c}(\xi) - \kappa),$$
$$F''(U_{\mu_c}(\xi)) = \delta'(U_{\mu_c}(\xi) - \kappa),$$
$$F'''(U_{\mu_c}(\xi)) = \delta''(U_{\mu_c}(\xi) - \kappa),$$

where the prime denotes differentiation with respect to the argument, and the identities

$$\int \delta(f(x))g(x)dx = \sum_{i=1}^{N} \frac{1}{|f'(x_i)|} \int \delta(x-x_i)g(x)dx,$$
$$\int \delta'(f(x))g(x)dx = -\int \delta(f(x)) \frac{d}{dx}\left[\frac{g(x)}{f'(x)}\right] dx,$$
$$\int \delta''(f(x))g(x)dx = \int \delta(f(x)) \frac{d}{dx}\left[\frac{1}{f'(x)}\frac{d}{dx}\left[\frac{g(x)}{f'(x)}\right]\right] dx,$$

with $f(x_i) = 0$ for $i = 1, \ldots, N$ [24]. We then have that

$$\mathcal{K}_1(\sin^2(2\theta)) = \frac{2\sin^2(2\Delta_{\mu_c})}{\Gamma} = \frac{1}{w_2 \widetilde{J}_{\mu_c}(0)}$$

and

$$\partial_\mu \mathcal{I}(\cos(k_c x))\big|_{\mu=\mu_c} = \frac{1}{\sqrt{2\pi}} \int_{-\infty}^{\infty} e^{-x^2/2\sigma^2} \cos^2(px) = \frac{\sigma}{2}\left(e^{-2\sigma^2 p^2} + 1\right).$$

Therefore we obtain

$$\gamma = \frac{\sigma(e^{-2\sigma^2 p^2}+1)}{2\widetilde{J}_{\mu_c}(0)}$$

so that $\gamma > 0$ since $\widetilde{J}_{\mu_c}(0) > 0$.

Next we have that

$$\begin{aligned}\mathcal{K}_3(\sin(2\theta)) =& \frac{1}{8w_2^3 \widetilde{J}_{\mu_c}(0)^3 \sin^4(2\Delta_{\mu_c})} \times \left[\partial_\theta\left(\frac{1}{\sin(2\theta)}\partial_\theta\left(\sin^3(2\theta)\right)\right)\Big|_{\theta=\Delta_{\mu_c}}\right. \\ &\left. + \partial_\theta\left(\frac{1}{\sin(2\theta)}\partial_\theta\left(\sin^3(2\theta)\right)\right)\Big|_{\theta=\Delta_{\mu_c}}\right] \\ =& \frac{3\cos(4\Delta_{\mu_c})}{w_2^3 \widetilde{J}_{\mu_c}(0)^3 \sin^4(2\Delta_{\mu_c})}\end{aligned}$$

and

$$\mathcal{I}(\cos(k_c x)) = \widetilde{J}_{\mu_c}(k_c) = \widetilde{J}_{\mu_c}(0),$$

since this was the condition for the bifurcation. Therefore

$$C_1 = \frac{9\cos(4\Delta_{\mu_c})}{4w_2^2 \widetilde{J}_{\mu_c}(0)^2 \sin^4(2\Delta_{\mu_c})}.$$

Next we compute $u_2(x,\theta,\tau)$. Recall that

$$u_2(x,\theta,\tau) = \frac{1}{2} z(\tau)^2 \left[A_0 + A_2\cos(2\theta) + (\widetilde{A}_0 + \widetilde{A}_2\cos(2\theta))\cos(2k_c x)\right],$$

where the coefficients are determined by (2.38) and (2.39). We first must compute the functionals

$$\mathcal{K}_1(1) = \frac{2}{\Gamma}, \quad \mathcal{K}_1(\cos(2\theta)) = \frac{2\cos(2\Delta_{\mu_c})}{\Gamma}, \quad \mathcal{K}_1(\cos^2(2\theta)) = \frac{2\cos^2(2\Delta_{\mu_c})}{\Gamma}$$

and, on setting $\widetilde{J}_{\mu_c}(nk_c) = \widetilde{J}_n$,

$$\begin{aligned}
\mathcal{K}_2(1) &= \frac{1}{2w_2\widetilde{J}_0 \sin(2\Delta_{\mu_c})\Gamma}\left[\partial_\theta(\sin(2\theta))\Big|_{\theta=\Delta_{\mu_c}} + \partial_\theta(\sin(2\theta))\Big|_{\theta=-\Delta_{\mu_c}}\right] \\
&= \frac{2\cos(2\Delta_{\mu_c})}{w_2\widetilde{J}_0 \sin(2\Delta_{\mu_c})\Gamma}, \\
\mathcal{K}_2(\cos(2\theta)) &= \frac{1}{2w_2\widetilde{J}_0 \sin(2\Delta_{\mu_c})\Gamma} \\
&\quad \times \left[\partial_\theta(\cos(2\theta)\sin(2\theta))\Big|_{\theta=\Delta_{\mu_c}} + \partial_\theta(\cos(2\theta)\sin(2\theta))\Big|_{\theta=-\Delta_{\mu_c}}\right] \\
&= \frac{2\cos(4\Delta_{\mu_c})}{w_2\widetilde{J}_0 \sin(2\Delta_{\mu_c})\Gamma}.
\end{aligned}$$

Plugging these into (2.38) and (2.39) yields

$$\begin{aligned}
A_0 &= -\frac{w_0 \sin(8\Delta_{\mu_c})}{4w_2\widetilde{J}_0 \sin^4(2\Delta_{\mu_c})w(2\Delta_{\mu_c})}, \\
A_2 &= \frac{2w_0 + w_2 + (6w_0 - 2w_2)\cos(4\Delta_{\mu_c}) + w_2\cos(8\Delta_{\mu_c})}{8w_2\widetilde{J}_0 \sin^4(2\Delta_{\mu_c})w(2\Delta_{\mu_c})}.
\end{aligned}$$

Moreover, noting that

$$\mathcal{I}(\cos(2k_c x)) = \widetilde{J}_2,$$

we have

$$\begin{aligned}
\widetilde{A}_0 &= \frac{w_0\widetilde{J}_2(\widetilde{J}_2 - \widetilde{J}_0 + (\widetilde{J}_0 + 3\widetilde{J}_2)\cos(4\Delta_{\mu_c}))\cos(2\Delta_{\mu_c})}{4\widetilde{J}_0^2 w_2 \sin^3(2\Delta_{\mu_c})(\widetilde{J}_0 w_2 \sin^2(2\Delta_{\mu_c}) - \widetilde{J}_2 w_2\cos^2(2\Delta_{\mu_c}) - \widetilde{J}_2 w_0)}, \\
\widetilde{A}_2 &= \frac{-\widetilde{J}_2(\widetilde{J}_2 w_0\cos^2(2\Delta_{\mu_c}) + \cos(4\Delta_{\mu_c})(\widetilde{J}_2 w_0 - \widetilde{J}_0 w_2 \sin^2(2\Delta_{\mu_c})))}{2\widetilde{J}_0^2 w_2 \sin^3(2\Delta_{\mu_c})(\widetilde{J}_0 w_2 \sin^2(2\Delta_{\mu_c}) - \widetilde{J}_2 w_2\cos^2(2\Delta_{\mu_c}) - \widetilde{J}_2 w_0)}.
\end{aligned}$$

Therefore, computing the terms from the quadratic form, we have

$$\begin{aligned}
B_1 &= -\frac{\cos(4\Delta_{\mu_c})}{2w_2^2\widetilde{J}_0^3 \sin^4(2\Delta_{\mu_c})}, \\
B_2 &= \frac{\widetilde{J}_2(w_0(\widetilde{J}_2 - \widetilde{J}_0 - (\widetilde{J}_0 - 3\widetilde{J}_2\cos(4\Delta_{\mu_c})) + 2w_2\widetilde{J}_0\cos^2(4\Delta_{\mu_c})))}{4\widetilde{J}_0^4 w_2^2 \sin^4(2\Delta_{\mu_c})(\widetilde{J}_0 w_2 \sin^2(2\Delta_{\mu_c}) - \widetilde{J}_2 w_2\cos^2(2\Delta_{\mu_c}) - \widetilde{J}_2 w_0)}.
\end{aligned}$$

Since we are only interested in the sign of β we can obtain an inequality for B_2 by noting that

$$\widetilde{J}_0 w_2 \sin^2(2\Delta_{\mu_c}) - \widetilde{J}_2 w_2\cos^2(2\Delta_{\mu_c}) - \widetilde{J}_2 w_0 > -\widetilde{J}_0 w(2\Delta_{\mu_c}) > 0,$$

where we have used the fact that $\widetilde{J}(0) > \widetilde{J}(2k_c)$ and $w_2 > w_0$. Additionally we have

$$\begin{aligned}
&w_0(\widetilde{J}_2 - \widetilde{J}_0 - (\widetilde{J}_0 - 3\widetilde{J}_2)\cos(4\Delta_{\mu_c})) + 2w_2\widetilde{J}_0\cos^2(4\Delta_{\mu_c}) \\
&< -3w_2\widetilde{J}_0\cos(4\Delta_{\mu_c}),
\end{aligned}$$

so that

$$B_2 < \frac{3\widetilde{J}_2 \cos(4\Delta_{\mu_c})}{4\widetilde{J}_0^4 w_2 \sin^4(2\Delta_{\mu_c}) w(2\Delta_{\mu_c})}$$

and therefore

$$\begin{aligned}\beta &= \frac{1}{2}(B_1 + B_2) + \frac{1}{6}C_1 \\ &< \frac{(2\widetilde{J}_0 w(2\Delta_{\mu_c}) + 3\widetilde{J}_2 w_2)\cos(4\Delta_{\mu_c})}{16\widetilde{J}_0^4 w_2^2 \sin^4(2\Delta_{\mu_c}) w(2\Delta_{\mu_c})} \\ &\approx \frac{\cos(4\Delta_{\mu_c})}{8\widetilde{J}_0^3 w_2^2 \sin^4(\Delta_{\mu_c})}\end{aligned}$$

since $\widetilde{J}_2 \ll \widetilde{J}_0$. We then see that β has the same sign as $\cos(4\Delta_{\mu_c})$, which we know to be negative since $w(2\Delta_{\mu_c}) = w_0 + w_2 \cos(4\Delta_{\mu_c}) < 0$ and $w_0, w_2 > 0$. Thus we have that the amplitude equation is given by

$$\frac{dz}{dt} = \gamma \Delta\mu z + \beta z^3$$

with $\gamma > 0$ and $\beta < 0$, so that the amplitude undergoes a supercritical pitchfork bifurcation.

REFERENCES

[1] S. Amari, *Dynamics of pattern formation in lateral inhibition type neural fields*, Biol. Cybern., 27 (1977), pp. 77–87.

[2] A. Angelucci, J. B. Levitt, E. J. S. Walton, J.-M. Hupe, J. Bullier, and J. S. Lund, *Circuits for local and global signal integration in primary visual cortex*, J. Neurosci., 22 (2002), pp. 8633–8646.

[3] R. Ben-Yishai, R. L. Bar-Or, and H. Sompolinsky, *Theory of orientation tuning in visual cortex*, Proc. Natl. Acad. Sci. USA, 92 (1995), pp. 3844–3848.

[4] G. G. Blasdel, *Orientation selectivity, preference, and continuity in monkey striate cortex*, J. Neurosci., 12 (1992), pp. 3139–3161.

[5] G. G. Blasdel and G. Salama, *Voltage-sensitive dyes reveal a modular organization in monkey striate cortex*, Nature, 321 (1986), pp. 579–585.

[6] T. Bonhoeffer and A. Grinvald, *Orientation columns in cat are organized in pinwheel like patterns*, Nature, 364 (1991), pp. 166–146.

[7] P. C. Bressloff, *Traveling fronts and wave propagation failure in an inhomogeneous neural network*, Phys. D, 155 (2001), pp. 83–100.

[8] P. C. Bressloff, *Spatially periodic modulation of cortical patterns by long-range horizontal connections*, Phys. D, 185 (2003), pp. 131–157.

[9] P. C. Bressloff, *Spatio-temporal dynamics of continuum neural fields*, J. Phys. A, 45 (2012), 033001.

[10] P. C. Bressloff, *Waves in Neural Media: From Single Neurons to Neural Fields*, Springer, 2014.

[11] P. C. Bressloff and J. D. Cowan, *Amplitude equation approach to contextual effects in visual cortex*, Neural Comput., 14 (2002), pp. 493–525.

[12] P. C. Bressloff, J. D. Cowan, M. Golubitsky, and P. J. Thomas, *Scalar and pseudoscalar bifurcations: Pattern formation on the visual cortex*, Nonlinearity, 14 (2001), pp. 739–775.

[13] P. C. Bressloff, J. D. Cowan, M. Golubitsky, P. J. Thomas, and M. Wiener, *Geometric visual hallucinations, Euclidean symmetry and the functional architecture of striate cortex*, Phil. Trans. Roy. Soc. Lond. B, 356 (2001), pp. 299–330.

[14] P. C. Bressloff and M. Webber, *Neural field model of binocular rivalry waves*, J. Comput. Neurosci., 32 (2012), pp. 233–252.

[15] P. C. Bressloff and M. A. Webber, *Front propagation in stochastic neural fields*, SIAM J. Appl. Dyn. Syst., 11 (2012), pp. 708–740.
[16] M. Camperi and X.-J. Wang, *A model of visuospatial short-term memory in prefrontal cortex: Recurrent network and cellular bistability*, J. Comput. Neurosci., 5 (1998), pp. 383–405.
[17] R. D. Chervin, P. A. Pierce, and B. W. Connors, *Periodicity and directionality in the propagation of epileptiform discharges across neocortex*, J. Neurophysiol., 60 (1988), pp. 1695–1713.
[18] P. Chossat, G. Faye, and O. Faugeras, *Bifurcation of hyperbolic planforms*, J. Nonlinear Sci., 21 (2011), pp. 465–498.
[19] S. Coombes, *Waves, bumps and patterns in neural field theories*, Biol. Cybern., 93 (2005), pp. 91–108.
[20] S. Coombes, H. Schmidt, and I. Bojak, *Interface dynamics in planar neural field models*, J. Math. Neurosci., 2 (2012).
[21] G. B. Ermentrout, *Neural networks as spatio-temporal pattern-forming systems*, Rep. Progr. Phys., 61 (1998), pp. 353–430.
[22] G. B. Ermentrout and J. Cowan, *A mathematical theory of visual hallucination patterns*, Biol. Cybern., 34 (1979), pp. 137–150.
[23] G. B. Ermentrout and J. B. McLeod, *Existence and uniqueness of travelling waves for a neural network*, Proc. Roy. Soc. Edinburgh Sect. A, 123 (1993), pp. 461–478.
[24] S. E. Folias, *Nonlinear analysis of breathing pulses in a synaptically coupled neural network*, SIAM J. Appl. Dyn. Syst., 10 (2011), pp. 744–787.
[25] S. E. Folias and P. C. Bressloff, *Breathing pulses in an excitatory neural network*, SIAM J. Appl. Dyn. Syst., 3 (2004), pp. 378–407.
[26] S. E. Folias and P. C. Bressloff, *Breathers in two-dimensional neural media*, Phys. Rev. Lett., 95 (2005), 208107.
[27] J. M. Fuster and G. Alexander, *Neuron activity related to short-term memory*, Science, 173 (1971), pp. 652–654.
[28] M. A. Geise, *Neural Field Theory for Motion Perception*, Kluwer Academic, Dordrecht, 1999.
[29] X. Huang, W. C. Troy, Q. Yang, H. Ma, C. R. Laing, S. J. Schiff, and J. Wu, *Spiral waves in disinhibited mammalian neocortex*, J. Neurosci., 24 (2004), pp. 9897–9902.
[30] D. H. Hubel and T. N. Wiesel, *Sequence regularity and geometry of orientation columns in the monkey striate cortex*, J. Comput. Neurol., 158 (1974), pp. 267–294.
[31] D. H. Hubel and T. N. Wiesel, *Uniformity of monkey striate cortex: A parallel relationship between field size, scatter, and magnification factor*, J. Comput. Neurol., 158 (1974), pp. 295–306.
[32] Z. P. Kilpatrick and B. Ermentrout, *Wandering bumps in stochastic neural fields*, SIAM J. Appl. Dyn. Syst., 12 (2013), pp. 61–94
[33] C. R. Laing, W. C. Troy, B. Gutkin, and G. B. Ermentrout, *Multiple bumps in a neuronal model of working memory*, SIAM J. Appl. Math., 63 (2002), pp. 62–97.
[34] S. LeVay and S. B. Nelson, *Columnar organization of the visual cortex*, in The Neural Basis of Visual Function, A. G. Leventhal, ed., CRC Press, Boca Raton, FL, 1991, pp. 266–315.
[35] D. J. T. Liley, P. J. Cadusch, and M. P. Dafilis, *A spatially continuous mean field theory of electrocortical activity*, Network, 13 (2002), pp. 67–113.
[36] P. I. Nunez, *Neocortical Dynamics and Human EEG Rhythms*, Oxford University Press, New York, 1995.
[37] K. Obermayer and G. G. Blasdel, *Geometry of orientation and ocular dominance columns in monkey striate cortex*, J. Neurosci., 13 (1993), pp. 4114–4129.
[38] D. J. Pinto and G. B. Ermentrout, *Spatially structured activity in synaptically coupled neuronal networks:* I. *Traveling fronts and pulses*, SIAM J. Appl. Math., 62 (2001), pp. 206–225.
[39] D. Pinto, S. L. Patrick, W. C. Huang, and B. W. Connors, *Initiation, propagation, and termination of epileptiform activity in rodent neocortex in vitro involve distinct mechanisms*, J. Neurosci., 25 (2005), pp. 8131–8140.
[40] J. Rankin, A. I. Meso, G. S. Masson, O. Fuageras, and P. Kornprobst, *Bifurcation study of a neural field competition model with an application to perceptual switching in motion integration*, J. Comput. Neurosci., 36 (2014), pp. 193–213.
[41] K. A. Richardson, S. J. Schiff, and B. J. Gluckman, *Control of traveling waves in the mammalian cortex*, Phys. Rev. Lett., 94 (2005), 028103.
[42] P. A. Robinson, C. J. Rennie, J. J. Wright, H. Bahramali, E. Gordon, and D. I. Rowe, *Pre-*

diction of electroencephalographic spectra from neurophysiology, Phys. Rev. E, 63 (2001), 021903.
[43] A. Sarti, G. Citti, and J. Petitot, *The symplectic structure of the primary visual cortex*, Biol. Cybern., (2008), pp. 33–48.
[44] L. Schwabe, K. Obermayer, A. Angelucci, and P. C. Bressloff, *The role of feedback in shaping the extra-classical receptive field of cortical neurons: A recurrent network model*, J. Neurosci., 26 (2006), pp. 9117–9129.
[45] E. Schwartz, *Spatial mapping in the primate sensory projection: Analytic structure and relevance to projection*, Biol. Cybern., 25 (1977), pp. 181–194.
[46] D. C. Somers, S. Nelson, and M. Sur, *An emergent model of orientation selectivity in cat visual cortical simple cells*, J. Neurosci., 15 (1995), pp. 5448–5465.
[47] H. Sompolinsky and R. Shapley, *New perspectives on the mechanisms for orientation selectivity*, Curr. Opin. Neurobiol., 5 (1997), pp. 514–522.
[48] M. L. Steyn-Ross, D. A. Steyn-Ross, J. W. Sleigh, and D. R. Whiting, *Theoretical predictions for spatial covariance of the electroencephalographic signal during the anesthetic-induced phase transition: Increased correlation length and emergence of spatial self-organization*, Phys. Rev. E, 68 (2003), 021902.
[49] N. V. Swindale, *The development of topography in the visual–cortex: A review of models*, Network, 7 (1996), pp. 161–274.
[50] J. S. Taube and J. P. Bassett, *Persistent neural activity in head direction cells*, Cereb. Cortex, 13 (2003), pp. 1162–1172.
[51] X.-J. Wang, *Synaptic reverberation underlying mnemonic persistent activity*, Trends Neurosci., 24 (2001), pp. 455–463.
[52] M. A. Webber and P. C. Bressloff, *The effects of noise on binocular rivalry waves: A stochastic neural field model*, J. Stat. Mech., 3 (2013), P03001.
[53] H. R. Wilson, R. Blake, and S. H. Lee, *Dynamics of traveling waves in visual perception*, Nature, 412 (2001), pp. 907–910.
[54] H. R. Wilson and J. D. Cowan, *Excitatory and inhibitory interactions in localized populations of model neurons*, Biophys. J., 12 (1972), pp. 1–23.
[55] H. R. Wilson and J. D. Cowan, *A mathematical theory of the functional dynamics of cortical and thalamic nervous tissue*, Kybernetik, 13 (1973), pp. 55–80.
[56] J. Wu, *Propagating waves of activity in the neocortex: What they are, what they do*, Neuroscientist, 14 (2008), pp. 487–502.
[57] K. Zhang, *Representation of spatial orientation by the intrinsic dynamics of the head-direction cell ensemble: A theory*, J. Neurosci., 16 (1996), pp. 2112–2126.